Dedicated to Professor Bernhard Wunderlich on the occasion of his 65th birthday

DYNAMIC DSC, SAXS AND WAXS ON HOMOGENEOUS ETHYLENE-PROPYLENE AND ETHYLENE-OCTENE COPOLYMERS WITH HIGH COMONOMER CONTENTS

V. B. F. Mathot[*#], *R. L. Scherrenberg*[*], *M. F. J. Pijpers*[*] *and W. Bras*[**]

[*]DSM Research, P. O. Box, 6160 MD Geleen
[**]Amolf, Kruislaan 407, 1098 SJ Amsterdam, The Netherlands

Abstract

Ethylene-propylene (EP) and ethylene-octene (EO) copolymers polymerized with the aid of homogeneous vanadium and metallocene catalysts were compared by DSC and time-resolved simultaneous SAXS-WAXS-DSC at scanning rates of 10 and 20°C min^{-1} using synchrotron radiation. An EP copolymer with a density of 896 kg m^{-3} (about 89 mol% ethylene) after compression moulding gave orthorhombic WAXS reflections. The crystallinity as a function of temperature [$w^c(T)$] calculated from these reflections using the two-phase model was in good agreement with $w^c(T)$ calculated from c_p measurements using DSC. The c_p measurements also enabled calculation of the baseline c_p and the excess c_p. The SAXS measurements revealed a strong change in the long period in cooling and in heating. The SAXS invariant as a function of temperature showed a maximum in both cooling and heating, which could be explained from the opposing influences of the crystallinity and the electron density difference between the two phases. Two EO copolymers with densities of about 871 kg m^{-3} (about 87 mol% ethylene) no longer showed any clear WAXS reflections, although DSC and SAXS measurements showed that these copolymers did crystallize. The similarity between the results led to the conclusion that the copolymers, though based on different catalyst systems – vanadium and metallocene – did not have strongly different sets of propagation probabilities of chain growth during polymerization. On the basis of a Monte Carlo simulation model of crystallization and morphology, based on detailed knowledge of the microchain structure, the difference between WAXS on the one hand and DSC and SAXS on the other could be explained as being due to loosely packed crystallized ethylene sequences in clusters. These do cause the density and the electron density of the cluster to increase (which is measurable by SAXS) and the enthalpy to decrease (which is measurable by DSC) but the clusters are too small and/or too imperfect to give constructive interference in the case of WAXS. Of an EP copolymer with an even lower ethylene content (about 69 mol%), the crystallization and melting processes could still be readily measured by DSC and SAXS, which proves that these techniques are eminently suitable for investigating the crystallization and melting behaviour of the copolymers studied.

Author to whom all correspondence should be addressed.

1. Introduction

Since the first low-density polyethylene, LDPE, was polymerized via a high-pressure process more than 50 years ago, a wide variety of polyethylene types has been developed. See Fig. 1 for an overview [1, 2].

Besides LDPE, which is still the most complex polyethylene in terms of molecular structure, linear polyethylene (LPE) and – via branching of the main chain – high density polyethylene (HDPE) have been developed. A recent development is ultra-high molecular weight polyethylene, UHMWPE, which has attracted a great deal of interest as base polymer for superstrong polyethylene fibres.

At the same time, by combining the simple building blocks ethylene, propylene, 1-butene and 1-octene a wide variety of copolymers have been developed over the years, with an equally wide variety of properties and applications. An important structural parameter in polymers, including ethylene copolymers, is the molar mass distribution. Not only does it largely determine the processabil-
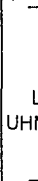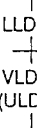
		Linear	Short Chain Branched		
			Homogeneous	Heterogeneous	
Crystalline	1000				Molar Mass Distribution
	970	LPE UHMWPE		UHMWPE HDPE	
Semi-crystalline			Ethylene Copolymers		Sample History
	920			LDPE (SCB+LCB) / LLDPE / VLDPE (ULDPE)	Ethylene Sequence Length Distribution
	880		EPDM		
Amorphous	855				
State at 25°C	D 25°C (kg/m³)		Single Peaked	Multiple Peaked	Influencing Thermal Properties
			DSC Curve Shape		

Fig. 1 Classification of important polyethylene types according to density at room temperature, chain structure, DSC-curve shape and parameters influencing the crystallization and melting behaviour

ity of a polymer in processes such as extrusion (another important parameter being long chain branching); it also definitely influences the mechanical properties, see for example [3]. In ethylene copolymers the microchain structure is also important [1, 4, 5]. First of all, the type of comonomer is an important variable [6–10]. Another important parameter when it comes to properties is the amount of comonomer incorporated into the chain. But the dominant influence is the specific arrangement of the comonomer groups in the chains [11–17].

Based on the latter parameter two important classes can be distinguished: homogeneous and heterogeneous short chain branched polyethylenes [1, 16]. Recently there has been a revival of the interest in homogeneous copolymers because of catalytic developments in this field. In particular by metallocene catalysis [18–23] in combination with specific polymerization processes a new class of homogeneous copolymers are currently being developed with properties different from those of the existing heterogeneous copolymers.

The degrees of freedom that a producer of ethylene copolymers has, are limited by the catalyst and the available process, such as a gas phase, solution, slurry or high-pressure process, and it is still difficult to manufacture 'tailor-made' copolymers. Within a particular process the polymerization conditions and the catalyst used largely determine the molecular structure of the product. This means that catalysis forms the key to the development of polymers with specific properties. In practice it is often attempted to influence the property profile directly via catalysis. The chance of success of such attempts can be increased by making use of the appropriate expertise.

In this connection it should be noted that it is important not only to determine the properties but also to unravel the molecular structure of the product and to study its crystallization behaviour and morphology [6, 24, 25]. In the case of end products, an additional requirement is that the processing step needs to be optimized in view of its large influence on the ultimate product properties via such aspects as specific rheology, crystallization under shear/pressure, orientation, etc.

Given the large number of variables that play a role, it is important that analytical tools be developed which can help steer the development of new types in a particular direction. Differential scanning calorimetry is one of the techniques that has served this purpose for years. The reason is that DSC is a readily manageable technique which in a short time can yield an impression of the (de)vitrification behaviour and the crystallization and melting behaviour [26]. These processes influence the properties of the product, in particular the mechanical properties. They are linked to the molecular structure because the latter not only determines the processing behaviour but also largely determines the (de)vitrification behaviour and the crystallization and melting behaviour. Furthermore, in a DSC experiment a sample can be subjected to any time/tem-

perature programme desired, which means this technique offers a unique opportunity to simulate practical conditions relating to both processing and properties.

Moreover, if sufficient information is available about the relationships between the various elements of the knowledge chain: molecular structure < > (de)vitrification, crystallization and melting during processing < > morphology < > properties, the DSC technique can be used as a fingerprinting technique for translating thermal properties into molecular structure (i.e. the route backwards along the knowledge chain).

The possibilities for clarifying the morphology element of the knowledge chain have recently been greatly enhanced by the development of high-intensity synchrotron radiation. The higher intensity (typically 10^5 times the intensity of conventional sources) shortens the required measuring time to such an extent that relatively fast crystallization and melting processes can be monitored. Below, 'dynamic' SAXS and WAXS measurements are reported which were taken during cooling and heating at 10 and 20°C min^{-1}, the same rates as used in DSC. This is a tremendous improvement compared with conventional, 'static', X-ray diffraction, where measuring times of the order of 1 hour are no exception. Such long measuring times give rise to all kinds of undesirable phenomena, such as annealing, reorganization, recrystallization, etc. The combination of DSC and SAXS-WAXS is thus a powerful tool for the study of crystallization, melting and morphology.

This article contains a report on research relating to the above-mentioned knowledge chain for homogeneous ethylene copolymers with propylene and octene as comonomers [27].

2. Experimental

2.1 Techniques

DSC

The measurements were performed with Perkin-Elmer differential scanning calorimeters, type DSC-7. The aluminium block surrounding the measuring unit was thermostatted by means of a metal buffer at −130°C. This thermostatting took place by means by a pulsating nitrogen supply from the CCA-7 cooling unit of Perkin Elmer. The cooling block of the thyristors of the DSC-7 was thermostatted at 15 to 20°C by a Lauda RM6 cooler. The measuring block and the glove box surrounding it were flushed with very dry nitrogen.

The temperature calibrations were made with the aid of the melting temperatures of pure indium, tin and lead at 5 and 20°C min^{-1}. The temperature correction for cooling rates was done by mirroring the corrections obtained in heating using an extrapolation to zero scanning rate. The temperature of the iso-

tropic $<>$ anisotropic transition of Azoxy anisole was used to check the calibration for both cooling and heating. The energy calibration was performed using the melting enthalpy of indium and was checked via c_p measurements of sapphire in the range measured. All calibrations were performed automatically by the software program. The sample masses were determined to the nearest µg.

The DSC-7 was linked on-line to a Hewlett-Packard 486/33M computer by an RS-232 interface. In-house developed software was used for measurement and evaluation. The digital temperature and measuring signal were scanned at a frequency of 4 Hz at maximum. In the dynamic range of $+/-$ 320 mW the signal could be measured within 1 µW. The noise was approx. $+/-1$ µW peak to peak.

SAXS-WAXS-DSC

Time-resolved simultaneous SAXS-WAXS-DSC measurements were performed on beam line 8.2 of the SRS at the SERC Daresbury Laboratory, Warrington, UK. The pin-hole camera was equipped with a multiwire quadrant detector (SAXS) located 3.5 metres from the sample position and a curved knife-edge detector (WAXS) that covered 120° of arc at a radius of 0.2 metre. The scattering pattern from an oriented specimen of wet collagen (rat-tail) was used to calibrate the SAXS detector and the reflections of an LLDPE were used to calibrate the WAXS detector. For a detailed description of the storage ring, radiation and camera geometry and data collection electronics, see earlier publications [28, 29]. The frames were taken at intervals of 1 and 2°C for the scanning rates of 10 and 20°C min^{-1} respectively. The experimental data were corrected for background scattering, sample transmission and the positional non-linearity of the detectors.

The DSC cell was a modified Linkam THM microscope hot stage, and was flushed with nitrogen. To enable the synchrotron beam to pass through the sample, the aluminium DSC pans were modified by punching holes in both the pan and the lid. These holes were covered with 0.025 mm thick mica windows which gave a negligible SAXS pattern and only discrete WAXS reflections which could be rotated out of the direction plane of the WAXS detector. The signal to noise ratio of the DSC curves obtained during the synchrotron experiments was inherently lower in comparison to a stand-alone DSC. Nevertheless, the simultaneous measurement of the DSC signal was very useful because it gave a good indication of and check on the thermal behaviour (via comparison with results of stand-alone DSC) of the sample and the temperature calibration during the experiment.

A measure of the variation of the crystallinity of EP copolymer EJ 207 as a function of temperature was obtained by determining the integrated intensity of

the WAXS 110 reflection after subtracting the amorphous contribution. For this purpose, the WAXS patterns of the EP copolymer EJ 198 were used after applying the same thermal treatment. In this way, the shift of the amorphous pattern with the temperature could be taken into account. The influence of the comonomer content is small [30].

The SAXS and WAXS patterns obtained were brought to an absolute scale via an external calibration at room temperature. For this purpose, the samples were given the same thermal history as during the synchrotron experiments. Subsequently, the samples were measured at room temperature on an Anton Paar Kratky type SAXS camera and a Philips PW 1820 Bragg-Brentano type goniometer. The absolute SAXS intensity of the sample was determined using a Lupolen standard, supplied with the Kratky camera. The absolute WAXS crystallinity was obtained by applying Ruland's method with a computer program developed by Vonk [31].

2.2 Samples

	Molecular structure data and densities of the ethylene-propylene and ethylene-1-octene copolymers						
Sample code	$D^{25°C}$ / kg m^{-3}	W_p or W_o / %	X_e / %	$[\eta]^{135°C}_{dec}$ / dl g^{-1}	M_n^* / kg mol^{-1}	M_w^* / kg mol^{-1}	M_z^* / kg mol^{-1}
EP EJ 207 Vanadium based	896	15.1	89.4	1.97	39	120	220
EO Vanadium based	872	34.2	88.5	3.04	130	240	380
EO Metallocene based	870	38.7	86.4	n.d.	42	91	150
EP EJ 198 Vanadium based	n.d.	40	69.2	3.15	105	270	470

Notes
* The asterisked M values were determined with the aid of SEC in 1,2,4 TCB at 135 or 150°C using universal calibration.
* Densities determined after compression moulding.
* W_p and W_o are the mass percentages of propylene and 1-octene, respectively; X_e is the molar percentage ethylene.
* n.d. = not determined

3. Results

3.1 Homogeneity and heterogeneity

Before specifically discussing homogeneous copolymers we should first place them in a broader context. In Fig. 1 the polyethylenes are characterized

in terms of chain structure, density and DSC curve shape. In addition, it is indicated which parameters influence the crystallization and melting processes.

Short chain branched (SCB) polyethylenes fall into two categories: homogeneous and heterogeneous. SCB may occur in the polyethylene chain due to a variety of causes, the most obvious one being copolymerization.

We speak of a *homogeneous copolymer* when the way in which the co-monomer is added during polymerization can be described by a single set of chain propagation probabilities of (co)monomer incorporation in the chain (*P* set), or alternatively, by the combination of a single set of reactivity ratios (*r* set) and a single monomer-comonomer ratio. Statistically there are no differences within and between molecules.

All other copolymers are *heterogeneous copolymers*. Two special, and extreme, cases are distinguished, viz. 'intramolecular heterogeneity' of co-monomer incorporation when the heterogeneity is manifested within the molecules, and 'intermolecular heterogeneity' when the heterogeneity is between molecules [1, 16, 32].

Figure 1 shows that the information about the molecular structure provided by DSC is unambiguous particularly when the DSC curve is multi-peaked, as in the case of linear low density polyethylene, LLDPE, and very low density polyethylene, VLDPE. It will be clear that it takes more than DSC alone to enable a distinction to be made between homogeneous ethylene copolymers on the one hand and heterogeneous polyethylenes such as HDPE and LDPE on the other if they have the same single-peaked DSC curve [33]. In particular a determination of the comonomer content and DSC measurements on fractions obtained via a separation according to molar mass are necessary in such cases [34].

Figure 2 shows DSC curves for a homogeneous and a heterogeneous ethylene-octene copolymer, referred to as EO and VLDPE, respectively [35].

The EO copolymer meets the definition of homogeneity given above in every respect, as the copolymer was made via polymerization with a (promoted) catalyst system consisting of an aluminium alkyl combined with a vanadium component [36–38]. The catalyst system used is known to have one active site. At a constant ethylene-octene feed during polymerization, this results in a statistical (not necessarily random) distribution of octene units in the chain. This leads to the occurrence of sequences of both octene and ethylene units. Since octenes and octene sequences greatly hinder crystallization – octene being excluded from the crystal – one may safely assume that upon cooling only the ethylene sequences can crystallize. According to generally accepted crystallization models, the ethylene sequence length distribution, ESLD, is modulated to a crystallite dimension distribution via crystallization. Thermodynamics dictate that upon heating in a DSC this results in a melting-point distribution, of which the DSC curve is a manifestation. The heat flow involved in melting is
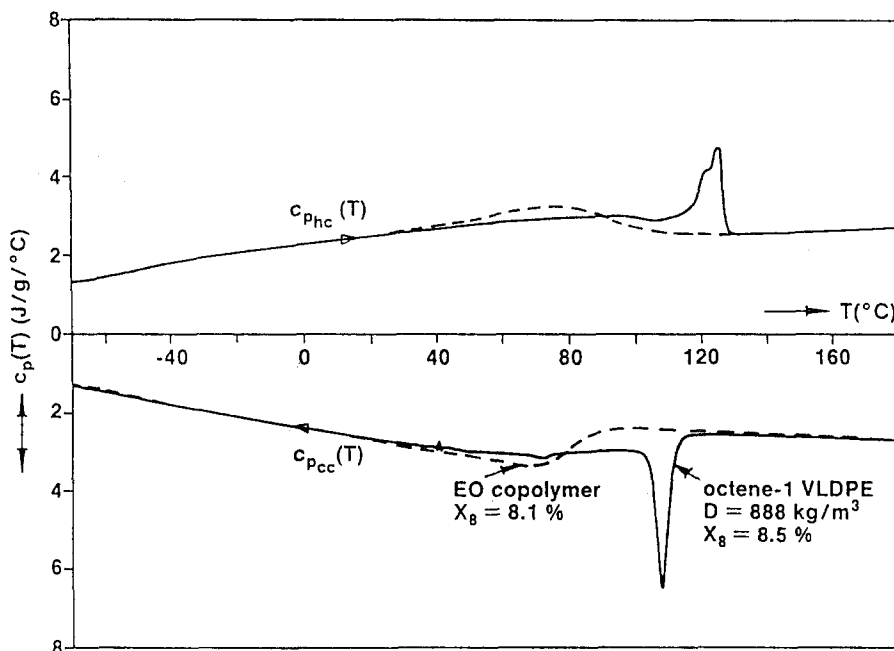
Fig. 2 DSC-2 continuous specific heat capacity curves at 10°C min^{-1} for a homogeneous
EO copolymer and a heterogeneous VLDPE. Cooling curve (downwards), $c_{pcc}(T)$,
and subsequent heating curve (upwards), $c_{phc}(T)$, in between –70 and 180°C. Isothermal stays of 5 min, sample masses of 9.259 mg (EO) and 10.005 mg (VLDPE)

then related to the number of sequences changing from the crystalline phase to
the melt phase. One can imagine that in this way a single-peaked ESLD can result in a single-peaked DSC curve via a single-peaked crystallite size distribution.

The same goes for the homogeneous copolymer prepared with the aid of a
metallocene catalyst, see 3.4. So it is definitely not true that the comonomers in
these copolymers are distributed over the chain in strictly regular fashion so
that ethylene sequences of equal length are formed. Like vanadium, the metallocene catalyst used in this case, too, is characterized by a statistical distribution
of the comonomers in each chain. Since the reactivity values may differ (but see
the notes in section 3.4!) from those of the vanadium catalyst, the resulting
ESLD may also differ, but will once again be single-peaked, as will the melting-point distribution measured with the aid of DSC.

Given the statistical character of comonomer addition, it is dangerous to
simply assume that in a homogeneous copolymer there is no difference between
the chains in terms of number and distribution of the comonomer units. Depending on the amount of incorporated comonomer and the chain length, there
may be differences. In the case of short chains and/or small quantities of incor-

porated comonomer differences due to (statistical) fluctuations are to be expected. In the case of the copolymers discussed here, however, the amounts of comonomer incorporated are so large that, statistically speaking, the chains will not differ much in terms of ESLD. This means that, as far as the role of individual chains is concerned, the only influence left is that of chain length on crystallization.

For LPE, HDPE, LDPE and copolymers with relatively low comonomer contents, chain length is an important parameter whose influence on crystallization is often greatly underestimated [5, 34, 39–46]. In the case of the copolymers to be reported on here, little is known about this influence. The influence of chain length is likely to be small when the ethylene sequences are very short, given the fact that heavily copolymerized chains in EPDM rubbers with the lowest densities, see Fig. 1, crystallize closest to the glass transition region. As a result, during crystallization from the melt the mobility of the chains and chain segments is progressively reduced. In such cases it is no longer very important whether the ethylene sequences are present in long or in short chains. Of course, this does not mean that chain length cannot have an influence under special conditions, such as crystallization in solution, in tension, under pressure, etc.

The VLDPE is an intermolecularly heterogeneous copolymer [35], for it has been found that the copolymer with 8.5 mol% octene in Fig. 2 can be separated into molecules with greatly varying comonomer contents. A crystallization-dissolution fractionation yielded fractions with widely different octene contents. More than half of the material (66% by mass; copolymer molecules which at room temperature are still in solution) has a very high – and still average – comonomer content (12.3 mol%) and can no doubt be split up further. The large variation in comonomer contents also explains the broad crystallization and melting range of about 200°C. VLDPEs illustrate the causal relationship between molecular structure, crystallization/melting and morphology very well, as their morphology, too, very clearly reflects their blend character [47–49]. For the sample in question, the chains with a high degree of comonomer incorporation form a continuous phase in which compact semi-crystalline domains (CSDs) can be distinguished which are composed of lamellae which vary greatly in length and thickness and consist of molecules with a lower degree of comonomer incorporation. The longest and thickest lamellae connect the CSDs and make it a co-continuous phase.

An obvious assumption in the case of VLDPE, and likewise in the case of LLDPE, is that the catalyst has two or more active sites which produce different types of chain (different in terms of comonomer incorporation). Given the multiple-peaked DSC curve, there must be a multiple-peaked crystallite distribution, which is caused by a multiple-peaked ESLD. In addition, other effects such as co-crystallization and recrystallization play a role, but this is also true for the homogeneous copolymer.

3.2 Homogeneous copolymers

In this section and the following homogeneous ethylene-propylene and ethylene-octene copolymers are discussed. The comonomers, propylene and octene, hinder crystallization in different ways and in this sense are opposites.

It is known that upon rapid crystallization of an ethylene-propylene copolymer, an isolated propylene unit in the polymer chain – a propylene which is flanked on both sides by many ethylene units – may be included to a certain extent as a defect in the ethylene crystal lattice at interstitional positions [50–55], although this is unfavourable from a thermodynamic point of view. If several propylene units lie in sequence, the chance of their being included in the ethylene crystal lattice as a defect is negligible. Isolated octenes, on the other hand, are not included in the crystal lattice as defects, or are included only to a very limited extent in the form of substitution defects [51–59]; octene sequences cannot be incorporated into the lattice. This means that in the case of ethylene-propylene copolymers the relationship between e.g. crystallization/ melting temperature and comonomer content will not be the same as in the case of ethylene-octene copolymers [5, 7].

In this connection it should be noted that when the comonomer content becomes very high the concepts of 'crystal lattice' and 'crystallites' need to be modified, see below.

The following sections contain the results of DSC and time-resolved simultaneous SAXS-WAXS-DSC experiments on a number of copolymers using synchrotron radiation. The aim is to illustrate to what extent these techniques can deepen our insight into the relationship between chain structure, crystallization and morphology rather than to give detailed relations for series of homogeneous copolymers. Besides, such series are rare, and this is in fact one of the reasons why opinions still differ about seemingly simple matters such as the relationships between comonomer content and crystallization/melting temperature, crystallinity etc.

The discussion below is divided into sections corresponding to density ranges. This is significant, since WAXS measurements on ethylene copolymers with different types of comonomers show that samples with densities above, say, 870 kg m^{-3} still have crystal reflections that can be measured reasonably well, while below this somewhat arbitrary density isotropic samples cooled from the melt at a rate of, say, 10°C min^{-1} no longer have such reflections. However, under special crystallization conditions, for example in tension or under pressure [60], things may be quite different.

In applying density as a distinguishing criterion one should be aware that in the case of copolymers the octene comonomer reduces the density more strongly than propylene. As can be seen in the table listing the sample data, the EP copolymer and the two EO copolymers all have about the same ethylene content, but the EO copolymers have substantially lower densities than the EP

copolymer. Besides in homogeneous copolymers the density is reduced much more effectively at the same ethylene content than in heterogeneous copolymers, see Fig. 2.

3.3 Homogeneous copolymers with densities of between about 870 and 900 kg m^{-3}

In the density range above 870 kg m^{-3} the possibilities offered by the above-mentioned techniques will be illustrated with reference to EJ 207, an ethylene-propylene copolymer containing 89.4 mol% ethylene and having a density after compression moulding of 896 kg m^{-3}.

EJ 207 is a homogeneous copolymer made via polymerization with a (promoted) catalyst system consisting of an aluminum alkyl combined with a vanadium component [36–38]. It has been proved possible to determine the chain structure of these copolymers with the aid of a specially developed polymerization model [61–63] based on the results of ^{13}C-NMR measurements [37, 64–66]. This determination was complicated by the fact that the propylene is incorporated into the chains in two different ways, viz. 'normally' and 'invertedly', which meant that a terpolymer model had to be used. The resultant first-order Markovian terpolymer model has recently been applied to vanadium based ethylene-octene copolymers as well [67], see the next section for such an EO copolymer. For the above-mentioned EP copolymers, the set of reactivity values for ethylene and the two types of propylene could be determined [61, 68], enabling the chain microstructures to be simulated in detail.

An example of such a simulation is given in Fig. 3a, showing a Monte Carlo simulation of part of a chain of EJ 207. The chain growth follows from the generation of random numbers between 0 and 1 and comparison of these with the P (propagation probability) values concerned. These probabilities P_{ij} relate to the addition of a j unit to a chain ending in an i unit, where both i and j may be ethylene, normal propylene or inverted propylene. In Fig. 3a a 'copolymer' representation is given in which no distinction is made between the two types of propylene. Because of the small number of units the statistics are not correct. Figure 3b shows the analytically calculated sequence length distributions for ethylene and propylene.

Figure 3a nevertheless gives a good impression of the distribution of propylenes and propylene sequences over a chain segment. It is not hard to imagine that these will hinder the crystallization of ethylene sequences in the chain segment.

Figure 4 shows the result of c_p measurements at 10°C min^{-1}. The figure includes the reference c_p curve for the purely amorphous phase, $c_{pa}(T)$, and the reference curve for the purely crystalline phase, $c_{pc}(T)$. For the latter the reference values as obtained for LPE were taken [69].

The $c_{pa}(T)$ values were obtained by extrapolation to the lowest temperatures of LPE melt data and paraffin data by means of Eq. (10) in [70]. At tempera-
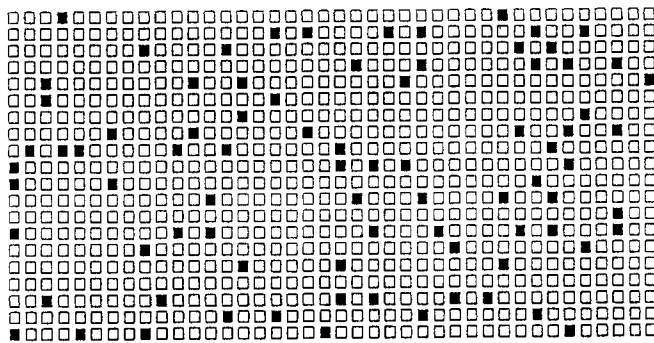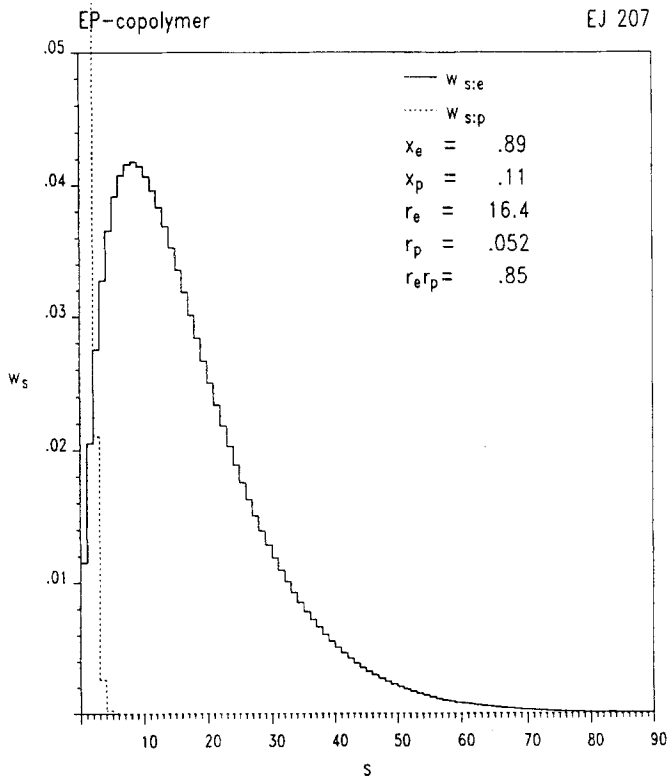
Fig. 3 a) Simulation of a segment of the chain for the EP copolymer EJ 207. The segment is constructed by linking the lines as in text reading; b) The mass fractions of ethylene in ethylene sequences of length s, $w_{s:e}$, and the mass fractions of propylene in propylene sequences of length s, $w_{s:p}$
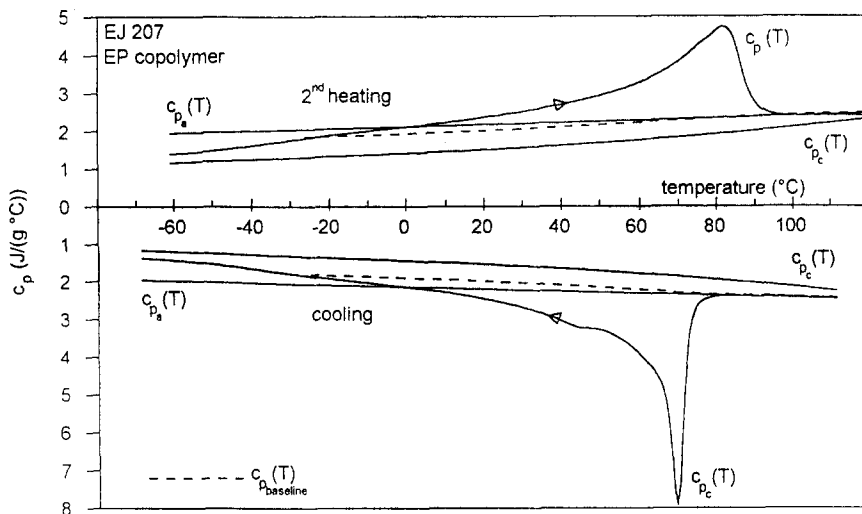
Fig. 4 DSC-7 continuous specific heat capacity curves, $c_p(T)$, at 10°C min^{-1} for EJ 207 obtained in cooling (downwards) and subsequent heating (upwards) in between –70 and 120°C; the reference curves, $c_{pa}(T)$ and $c_{pc}(T)$ and the baseline curves, $c_{pb}(T)$ (– – –). Isothermal stays of 5 min, sample mass of 13.547 mg

tures above 17°C the curve thus obtained coincides with that for LPE [69]. The choice of a $c_{pa}(T)$ deviating from that of LPE was made because the copolymers discussed here have a rather sharp glass transition (between about –60 and –40°C, in accordance with [71]). By contrast, LPE exhibits a gradual change in $c_{pa}(T)$ between –153 and 17°C, which may be interpreted as a continuous glass transition extending over a very wide temperature range. In this connection it is important to note that all our measurements on homogeneous and heterogeneous ethylene-propylene, ethylene-butene and ethylene-octene copolymers show full agreement between the $c_{pa}(T)$ used here and an experimental $c_{pa}(T)$, the latter being the part of a measured $c_p(T)$ curve above $T_{c,onset}$ and above $T_{m,end}$. This was true regardless of the comonomer content.

Figure 5 shows the enthalpy curves calculated via integration of the $c_p(T)$ measurements. The figure includes the reference enthalpy curves for the two extreme states, viz. the curves for purely amorphous LPE, $h_a(T)$, and purely crystalline LPE, $h_c(T)$. The cooling curve and the heating curve form a closed cycle.

Assuming the two-phase model to be valid for this copolymer, we may assume additivity of the enthalpy contributions for the two phases – amorphous and crystalline [72]

$$h(T) \equiv w^c(T)\, h_c(T) + w^a(T)\, h_a(T) \tag{1}$$

where

$$w^c(T) + w^a(T) = 1 \qquad (2)$$

With the aid of these two expressions we can define the enthalpy-based mass fraction crystallinity [72, 73], $w^c(T)$, below T_m^o, the equilibrium crystal-melt transition temperature:

$$w^c(T) = [h_a(T) - h(T)]/[h_a(T) - h_c(T)] \qquad (3)$$

Figure 9 shows the crystallinity curves calculated with the aid of (3) for cooling and heating based on the enthalpy curves in Fig. 5.
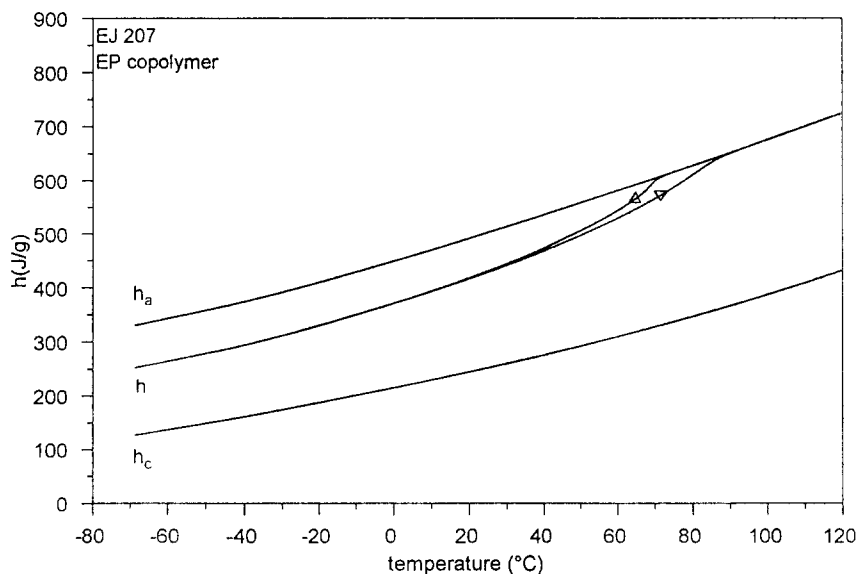

Fig. 5 Specific enthalpy cooling curve, subsequent heating curve and reference curves for EJ 207, based on the specific heat capacity curves shown in Fig. 4

Using the link between heat capacity and enthalpy we can define two important heat capacity functions [24, 72, 74, 75], viz. the baseline heat capacity and the excess heat capacity. Differentiation of $h(T)$ in (1) with respect to temperature

$$c_p(T) = (dh/dT)_p \qquad (4)$$

yields

$$c_p(T) = w^c(T)\, c_{pc}(T) + h_c(T)\, dw^c(T)/dT + w^a(T)\, c_{pa}(T) + h_a(T)\, dw^a(T)/dT \qquad (5)$$

$$= w^c(T)\, c_{pc}(T) + [1 - w^c(T)]\, c_{pa}(T) - [h_a(T) - h_c(T)]\, dw^c(T)/dT \qquad (6)$$

The $w(T)$ terms are regarded as belonging to the 'baseline' heat capacity and the $dw(T)/dT$ terms as belonging to the 'excess' heat capacity:

$$c_{pb}(T) \equiv w^c(T) \, c_{pc}(T) + [1 - w^c(T)]c_{pa}(T) \tag{7}$$

$$c_{pe}(T) \equiv -[h_a(T) - h_c(T)] \, dw^c(T)/dT \tag{8}$$

and

$$c_p(T) = c_{pb}(T) + c_{pe}(T) \tag{9}$$

The baseline heat capacity reflects the contributions of the temperature-dependent c_{pa} and c_{pc} to the experimental $c_p(T)$ via the crystallinity. In Fig. 4 the baseline heat capacities are shown for EJ 207 for cooling and for subsequent heating.

The excess heat capacity reflects contributions such as (re)crystallization, annealing and melting – processes by which the crystallinity is changed – to the experimental heat capacity. As has been stated in [72], the excess function is essential for the translation of a change in thermal properties of a material into a change in material structure or morphology, and the determination of $c_{pe}(T)$ is a real challenge.

The first part of the right-hand member of (8), the enthalpy reference differential function $h_a(T) - h_c(T) = \Delta h(T)$ [69, 72], is known for many polymers, see for example the ATHAS databank [76, 77]. The second part, the change in crystallinity with temperature $dw^c(T)/dT$, can be numerically calculated from $w^c(T)$, which function is given by (3).

The approach described here represents a clear and simple method for determining the baseline, provided that the two-phase model applies, of course. The intersection of a calculated baseline with a measured curve, see Fig. 4, may be said to mark the temperature:

– below which the crystallinity becomes constant so that the heat capacity virtually equals the baseline heat capacity: $c_p(T) \approx c_{pb}(T)$;

– and above which the crystallinity changes because excess phenomena play a role, which means there is a baseline heat capacity as well as an excess heat capacity: $c_p(T) =_s c_{pb}(T) + c_{pe}(T)$.

Clearly, the baseline is not a line one can simply draw by looking at the measured curve. Nor should this line be confused with the line which is obtained by extrapolating the part of the measured curve in the melt; in the case of the heating curve this is the part above the melting end temperature and in the case of the cooling curve it is the part above the onset of crystallization. As described earlier [72, 75] this line can be used to calculate the value of the numerator in (3). From this and $\Delta h(T)$, the denominator in (3), the crystallinity

curve can be calculated. Since it is not strictly necessary to carry out a heat capacity measurement in order to be able to extrapolate from the melt, this is also a practical method for quantitatively calculating the crystallinity curve from ordinary (but quantitative, due to correction for the empty-pan signal) DSC curves. It is even possible to calculate the excess $c_p(T)$ in this way without having to carry out a real heat capacity measurement [72, 75].

A method which is often used in practice involves drawing a straight line between two points (before and after the peak) of a measured curve and calculating a heat of crystallization or melting from the peak area between the curve measured and the line drawn. Obviously, this yields no more than a crude estimate, and it is not clear to what temperature the value found should be assigned. Moreover, the value found is operator-dependent. In short, this procedure does not result in a quantitative determination of the heat of crystallization, the heat of melting or the crystallinity as a function of temperature.

Incidentally, the approach presented here is not limited to the two-phase model but can be extended to a three-phase model [72, 78], for example if an interphase of rigid amorphous material [79–93] is present.

In the way described above the excess curves for EJ 207 as presented in Fig. 6 were calculated. As was already clear from Fig. 4, there is an excess heat capacity above approx. –20°C, which means that the sample is crystallizing and melting above this temperature.

The baseline and excess heat capacity curves and the crystallinity curves are highly sensitive to measuring errors on the one hand and the choice of reference curves on the other. Any inaccuracy in the DSC curve measured, for example an inaccuracy resulting from drift of the DSC, will immediately be reflected in, for example,

– the resulting curves no longer being 'closed' in the c_p, h, w^c and excess c_p plots, or

– the melt parts of the c_p no longer being symmetrical with respect to the temperature axis (reflexible in this axis), or

– the melt parts of the c_p curves not being consistent with the reference curve for $c_{pa}(T)$.

Clearly, it is very important to have good heat capacity and enthalpy reference curves. Therefore, the information available [76] should not only be continuously expanded but should also actually be used. To this end, producers of DSC equipment should incorporate this information into their software. In Fig. 4 the choice of $c_{pa}(T)$ for the copolymers discussed here was already briefly explained. This choice is not to be regarded as definitive, since for this type of copolymer a closer study of the location and width of the glass transition in dependence on the type, amount and distribution of comonomer is necessary.

Excess heat capacity curves as given in Fig. 6 serve as a starting point for the interpretation of DSC measurements in relation to the results of morphologi-
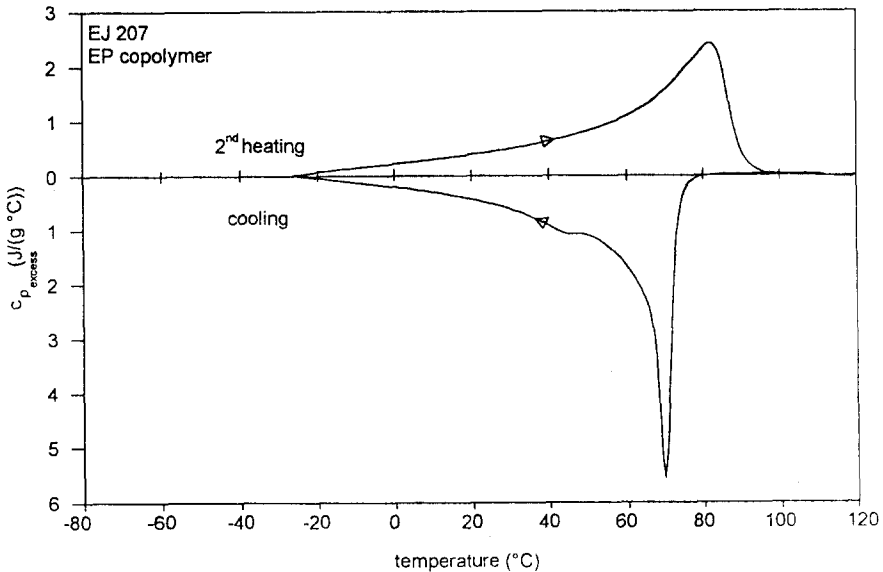
Fig. 6 Specific excess-heat capacity curves for EJ 207 for cooling and subsequent heating at 10°C min^{-1}

cal studies and, more specifically, as a starting point for the explanation of the crystallization and melting temperature distribution from the crystallite size distribution. Unfortunately, such measurements have very seldom been carried out until now, and have rarely been used [4, 72, 75].

Figure 7 shows the WAXS curves measured in the SAXS-WAXS-DSC set-up at the synchrotron facilities in Daresbury, UK. The curves were taken during cooling at a rate of 10°C min^{-1}. They show the formation of 110 and 200 reflections corresponding to the orthorhombic crystal structure of polyethylene below 80°C. It can be clearly seen that there is a continuous increase in intensity when going towards the lowest measuring temperature of –70°C. There are no indications of the presence of a triclinic or monoclinic phase.

On the basis of the simultaneously obtained SAXS curves, the so-called scattering invariant as a function of temperature was determined, see Fig. 8. This scattering invariant is given by integration in q of the absolute scattering intensity, $I(q,T)$:

$$Q(T) = \int_0^\infty I\,(q,\,T)q^2\mathrm{d}q \qquad (10)$$

where

$$q = 4\pi\sin\Theta/\lambda \qquad (11)$$

In the case of cooling a strong increase in the invariant is observed. Given the temperature at which this takes place, cf. the DSC cooling curve in Fig. 4 and the WAXS cooling curve in Fig. 7, it is clear that this increase is due to nucleation and crystallization. Compared with the DSC results, the increase in $Q(T)$ starts at somewhat lower temperatures. The heating curve (which is not shown here, but see for example the cooling and heating curves in Fig. 15) is also readily measurable, with clear hysteresis between crystallization and melting. For a two-phase system the invariant is described by

$$Q(T) = Cv^c(T) [1 - v^c(T)] [d_c(T) - d_a(T)]^2 \qquad (12)$$

where the constant C depends on the equipment used and represents the conversion factor from electron density (e mol cm^{-3}) to mass density (g cm^{-3}). The (volume) crystallinity $v^c(T)$ represents the fraction of crystalline phase with mass density $d_c(T)$; $1 - v^c(T)$ represents the fraction of amorphous phase with mass density $d_a(T)$.

It is important that in the calculation of the invariant according to (12) the temperature dependency of the mass densities and of the crystallinity is taken into account. Figure 8 includes, besides the experimental values of $Q(T)$ according to (10), calculated values according to (12). In the calculations the tem-
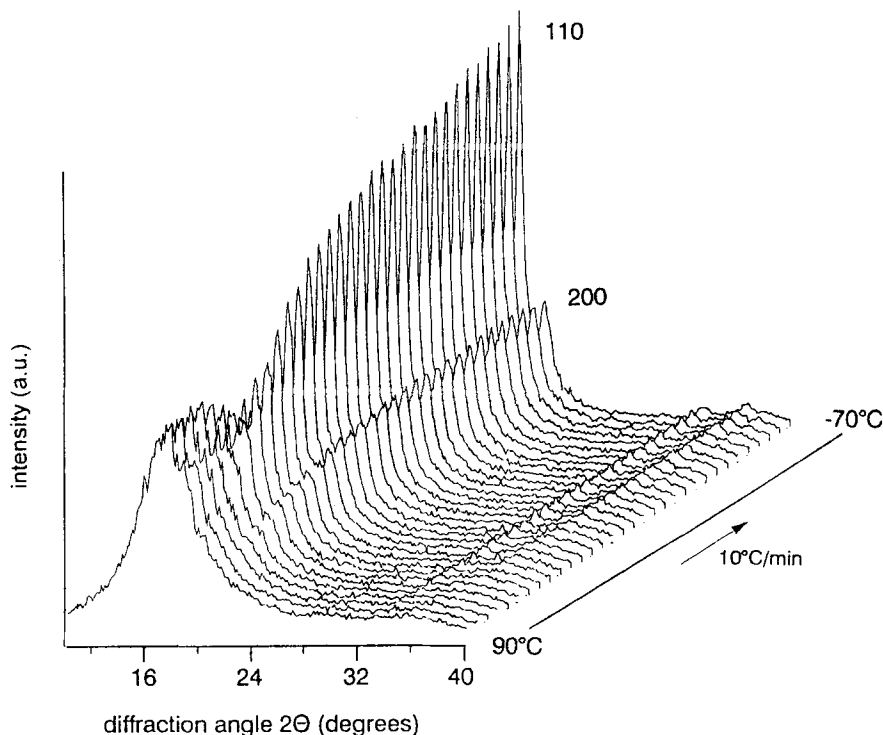

Fig. 7 WAXS curves for EJ 207, after 1 min waiting time at about 90°C, during cooling to about –70°C at 10°C min^{-1}
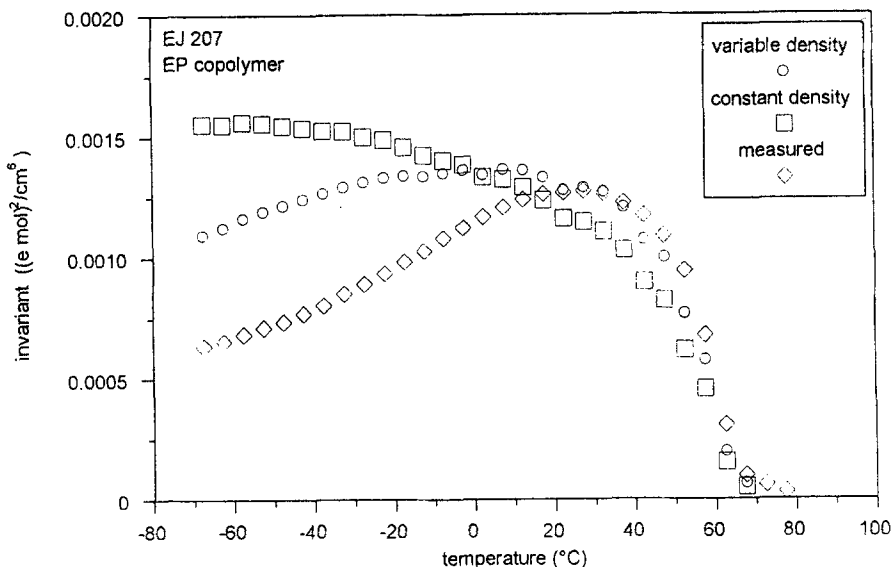
Fig. 8 SAXS measured and calculated invariant curves for EJ 207 during cooling from about 90 to about $-70°C$ at $10°C$ min^{-1}, see text for explanation of variable and constant density curves

perature-dependent values of the volume crystallinity were determined from the temperature-dependent mass crystallinities on the basis of the WAXS curves, see 2.1.

The invariant values labelled 'constant density' were subsequently calculated using constant values of d_a and d_c, viz. $d_a(T_R) = 855$ kg m^{-3} (the value for amorphous LPE at room temperature) and $d_c(T_R) = 1000$ kg m^{-3} (the value for crystalline LPE at room temperature). In Fig. 8 it can be seen that between 0 and $80°C$ the calculated values are still more or less in agreement with the measured values. As the temperature becomes lower, however, the calculated and measured values diverge more and more. Moreover, the calculated curve does not have the maximum characteristic of the copolymers under review. Incidentally, this maximum has nothing to do with the maximum given by the term $v^c(T)$ $[1 - v^c(T)]$ at $v^c(T) = 0.5$ [94]. After all, the crystallinities of the copolymers discussed here are all below 0.4. For this reason [and generally if $v^c(T)$ <0.5] the increase in $v^c(T)$ with decreasing temperature results in an increase in $Q(T)$ with decreasing temperature and cannot cause the maximum all by itself.

For the calculation labelled 'variable density' the same temperature-dependent values of the volume crystallinity were used. In this case, however, the temperature dependence of the densities was also taken into account, based on measurements by Swan and Wilski [95, 96]. The difference in density decreases with decreasing temperature. Since this density difference appears in the invariant formula as a square, any change in it has a significant influence. It is clear

that this trivial extension results in a curve which above 20°C is in excellent agreement with the measured curve. Moreover, this time the curve has a maximum. This maximum is the result of an increase in the product of $v^c(T)$ and $[1 - v^c(T)]$ and a decrease in $[d_c(T) - d_a(T)]^2$ with decreasing temperature. However, although the correction has led to an improved curve, the experimental values obtained between −70 and +20°C are still not described correctly. This contrasts with LLDPE, where the same approach did result in a correct description.

What could be the reason for this? In the first place, one might question the use of volume crystallinity values obtained by WAXS for calculating the invariant. Even in a perfect two-phase system, two different techniques need not yield the same crystallinities (and SAXS and WAXS are of course different in this respect!). In particular the size of the phase regions may play a role. This is clearly illustrated, see the following sections, by the fact that at high comonomer contents no WAXS reflections can be distinguished any more, while SAXS and DSC can still measure two separate states without any problem. For the sample discussed here, however, WAXS and DSC are still in good agreement, see Fig. 9, and particularly the temperature dependence is correct.

Apart from the fact that the phase domains are limited in size, as mentioned above, we may assume that the phases are not perfect. Not only will 'isolated' propylene units be included in the crystals as interstitial defects; as the crystallites become smaller (both in the direction of the ethylene sequences and perpendicular to this direction) the influence of the crystal surface, in particular the stress exerted on the crystallite core by the chains, will increase substantially.

Due to all these causes the density of the crystalline phase is likely to be lower than that of a purely crystalline LPE [Ref. [6] and references cited therein]. Lowering the density of the crystalline phase, and hence lowering the density difference in the formula for the invariant (12), results in a decrease in the calculated invariant values in the direction of the experimental values. Conversely, if 'good' crystallinity values were available, one could in principle calculate the density of the crystalline phase by fitting the measured values with (12). However, there are not enough morphology data available at present to enable such calculations to be made.

In Fig. 9 the (mass) crystallinity values as obtained with the aid of DSC and WAXS are compared. The WAXS crystallinity was determined as described in 2.1.

For this copolymer the crystallinities determined by DSC and by WAXS are in good agreement with one another, albeit that the WAXS cooling curve lies at slightly lower temperatures than that for DSC. In the case of both WAXS and DSC, the assumptions made with respect to the reference curves for the amorphous copolymer are uncertain factors. This means that it is well possible that
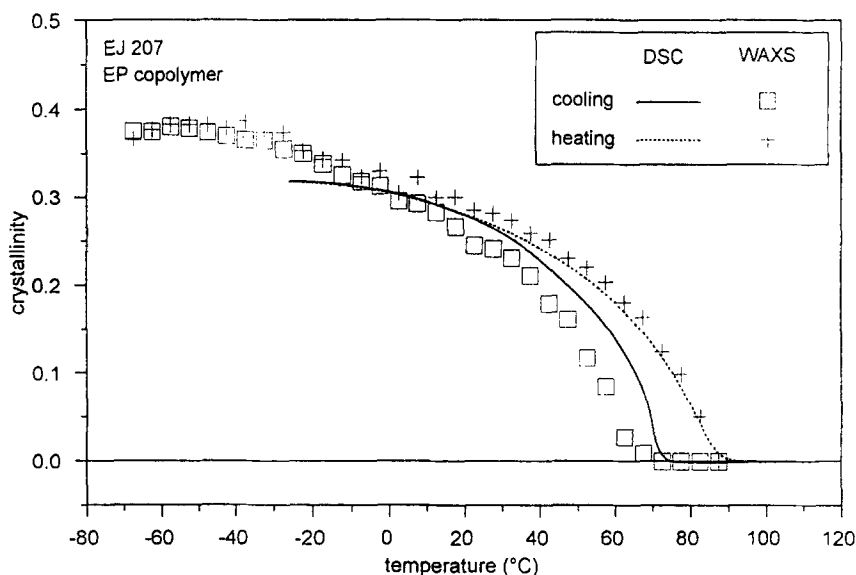
Fig. 9 Enthalpy-based mass crystallinity curves based on DSC en mass crystallinity curves from WAXS for cooling and subsequent heating at $10°C$ min^{-1} for EJ 207

instead of agreement with regard to the crystallinity a discrepancy is found. In other words, for this copolymer we could have used the temperature-dependent (volume) crystallinity based on DSC in calculating the invariant according to (12) without this giving essentially different results. It is striking that the WAXS crystallinity seems to increase even below $-20°C$, while according to DSC the sample starts to vitrify in that region. This is why the calculation of the DSC crystallinity was carried out up to and from the intersection of the baseline c_p and the measured c_p. At $-20°C$ we find for the DSC crystallinity about 32%. The mass crystallinity at room temperature calculated from $d = 896$ kg m^{-3} is 32%, which is slightly higher than the DSC value at room temperature. The difference in cooling rate ($10°C$ min^{-1} vs. cooling rate during compression moulding) is unlikely to be of influence here [2].

From the SAXS intensity curve for EJ 207 the long period can be calculated, for there is a clear maximum in $I(q,T)$. Within the two-phase system such an average periodic fluctuation of electron densities is interpreted in terms of an average distance between crystallites. Since transmission electron microscopy, after staining of the amorphous phase, reveals lamellae (not shown here) it is possible that at the highest temperature the average distance between the lamellae is responsible for the periodic fluctuation in electron densities.

As long as the TEM results and the SAXS results have not been compared in detail, we shall refrain from calculating an 'apparent amorphous dimension', L_a, and an 'apparent crystalline dimension', L_c, from the long period, L, according to the 'direct analysis':

$$L_a = (1 - v^c)L \qquad (13)$$

$$L_c = v^c L \qquad (14)$$

This is not because the two-phase model does not apply but because the direct method is based on a lamellar stack model, which does not apply in the case of the copolymers discussed here. In order to extract more information from the SAXS measurements, we need to determine the shape factor, $P(q)$, and the structure factor, $S(q)$, which together make up the scattering intensity $I(q,T)$ according to

$$I(q,T) = P(q,T)S(q,T) \qquad (15)$$

In particular the determination of the shape factor for the lamellae and the other crystallites is a problem, because the morphology is not known in detail.

Figure 10 shows the temperature dependence of the long period for cooling as well as heating. The relationship found is similar to that found in the case of a two-phase morphology of lamellar stacks [94]. This is probably due mainly to the comparable development of the 'apparent amorphous dimension' which dominates the long period.
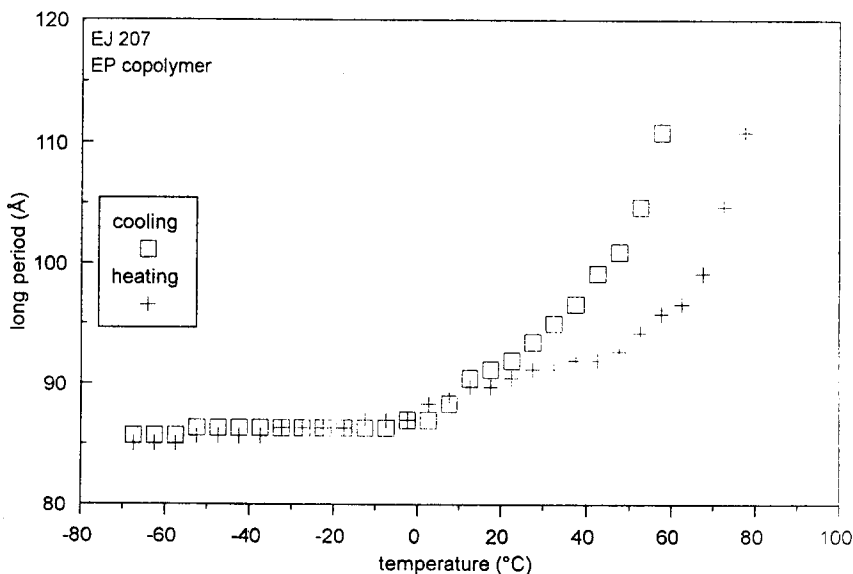

Fig. 10 The long period L as a function of temperature in cooling and subsequent heating at 10°C min^{-1} for EJ 207

3.4 Homogeneous copolymers with a density of about 870 kg m^{-3}

As noted in 3.2, octene reduces the density more effectively than propylene, see table with sample data. This is due not so much to a difference in the statis-

tics of comonomer incorporation but rather to the fact that it is virtually impossible for octene to be included in the crystal lattice, whereas propylene can readily be included. This means that in the case of ethylene-octene copolymers the ESLD has a much more dominant influence on crystallization because the hindering effect of octenes is much stronger.

Ethylene copolymers having a density after compression moulding of roughly 870 kg m^{-3} no longer show clear WAXS reflections, not even when cooled to −70°C, that is, not if they have been crystallized from an isotropic melt at atmospheric pressure. Figure 11 shows the WAXS curve at room temperature of the metallocene-based EO copolymer (86.4 mol% ethylene). The maximum is remarkably sharp. McFaddin et al. [30] reported a similar curve shape for an EO copolymer with 15 mol% octene. In Fig. 11, the 110 and 200 reflections are only vaguely distinguishable. This suggests a very low crystallinity, which however is not consistent with reality.
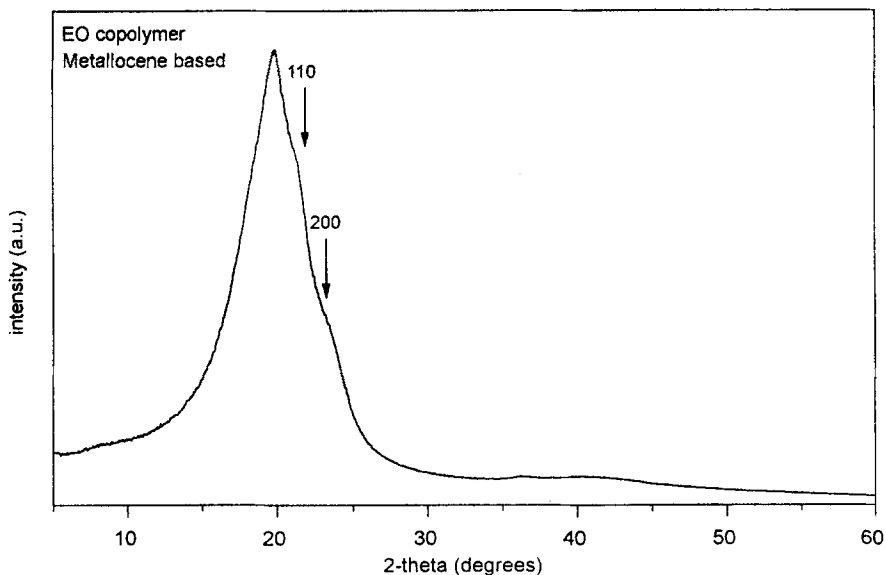

Fig. 11 WAXS curve for an EO copolymer after cooling from 150°C to room temperature at 20°C min^{-1}

Figure 12 convincingly shows this with reference to DSC curves for two ethylene-octene copolymers. For both copolymers, nucleation/crystallization in cooling starts at about 50°C and ends just above −50°C, where vitrification takes place. During heating from the glassy state, the copolymers are melting continuously up to about 90°C, where both melting ranges end. In the case of crystallization, the curves differ in the temperature range between about 10 and 50°C; the metallocene copolymer crystallizes first. This may be attributable to a difference in nucleation. Despite these differences, the area under the curves
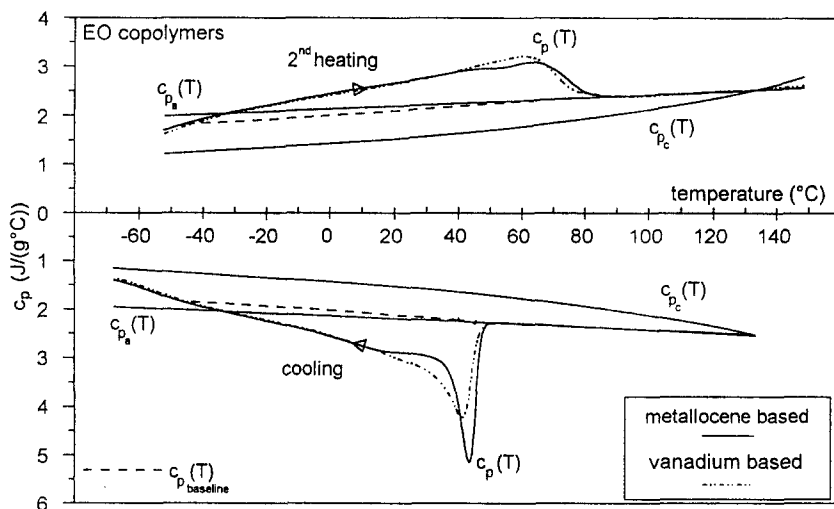
Fig. 12 DSC-7 continuous specific heat capacity curves, $c_p(T)$, at 20°C min^{-1} for two ethyl-
ene-octene copolymers produced with different catalyst systems. Cooling curves
(downwards) and subsequent heating curves (upwards) in between –70 and 150°C ;
the reference curves, $c_{pa}(T)$ and $c_{pc}(T)$ and the baseline curves, $c_{pb}(T)$ (– – –). Iso-
thermal stays of 5 min, sample masses of 10.646 mg (metallocene) and 9.892 mg
(vanadium)

is almost the same. Below 10°C the curves coincide. The differences with re-
gard to crystallization are not reproduced during the melting process upon heat-
ing. Apparently, they are eliminated by reorganization and annealing. This is
thus all the more reason to attribute the differences to nucleation rather than to
differences in molecular structure.

The EO copolymers were copolymerized with the aid of homogeneous cata-
lyst systems which were essentially different: one was a metallocene catalyst
and the other a vanadium-based catalyst, the same system as mentioned above
for the EP copolymer. It is remarkable that the DSC curves are not essentially
different. The comonomer contents are different (11.5 and 13.6%). Crystal-
lization and melting are mainly determined by differences in ESLD, especially
in the case of octene copolymers, assuming that for these copolymers the influ-
ence of molar mass is already limited. In the case of these two copolymers there
are apparently no essential differences in terms of ESLD, which means that the
P sets will not differ much. The fact that the ESLDs are similar at the given –
different – comonomer contents is an interesting observation, which might be
elaborated on by determining the sets of chain propagation probabilities (P sets)
for both systems. However, this would require copolymers with far higher co-
monomer contents to ensure that many methylene sequences are present which
are short enough to be measured by ^{13}C-NMR.

From the $c_p(T)$ curves the crystallinity curves are calculated with the aid of (3) as described above and indicated in Fig. 13. These curves, too, show hardly any difference, which confirms that the areas under the DSC curves are in
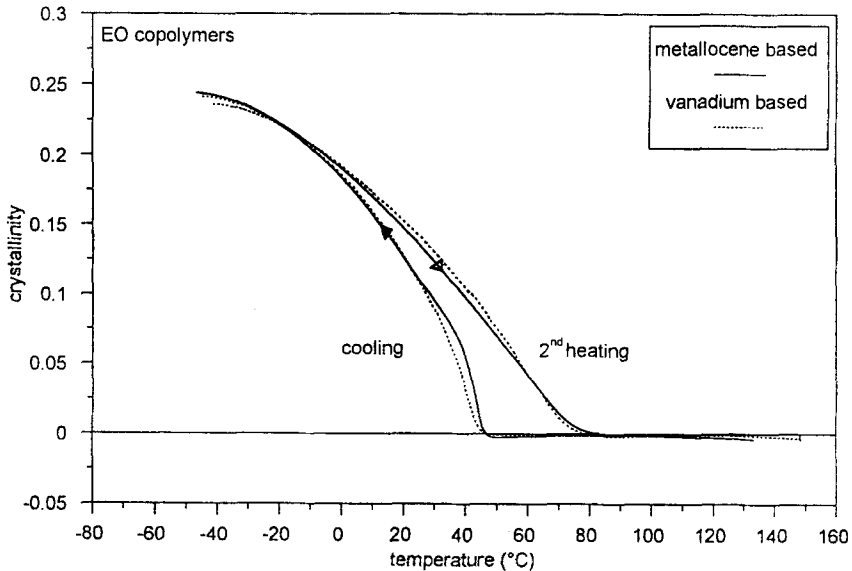

Fig. 13 Enthalpy-based mass crystallinity curves based on DSC for cooling and subsequent heating at $20°C$ min^{-1} for two EO copolymers, produced by different catalyst systems
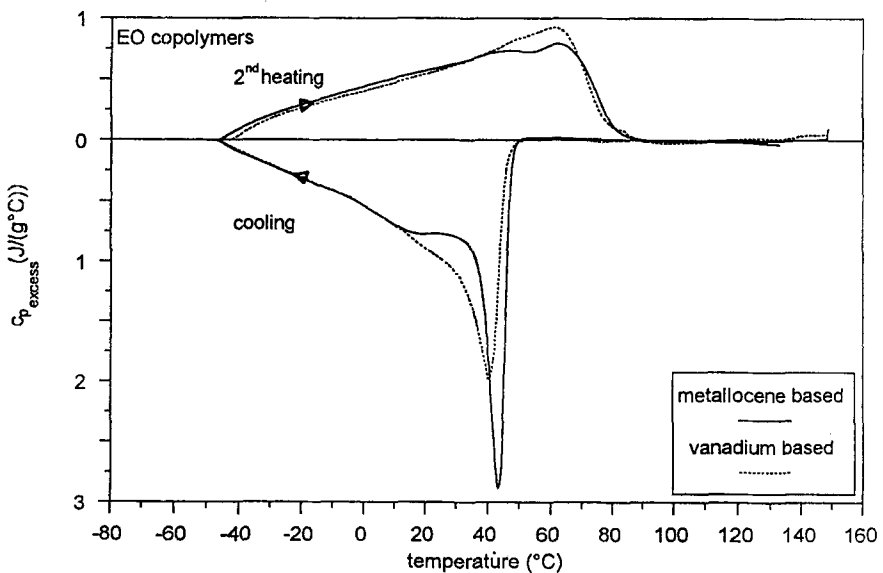

Fig. 14 Specific excess-heat capacity curves for cooling and subsequent heating at $20°C$ min^{-1} for two EO copolymers produced with the aid of different catalyst systems

agreement. As in Fig. 9, the data are plotted in such a way that apparently 'negative' and apparently 'positive' crystallinities in the melt can be shown, because this gives us an impression of the accuracy of the $c_p(T)$ measurements. After all, if $c_p(T)$ deviates in any way from $c_{pa}(T)$ in the melt, this deviation will be reproduced in magnified form in the $w^c(T)$ plot. As can be seen, the quality of the measurements is quite satisfactory. The maximum crystallinity at the lowest temperature is about 24%, which in absolute terms is about 8% lower than the DSC crystallinity for the EP copolymer EJ 207, see Fig. 9. Once again, the mass crystallinities, 14% and 12%, calculated from the densities of the copolymers, 872 and 870 kg m^{-3}, respectively, are in good agreement with the DSC crystallinities at room temperature.

The excess functions in Fig. 14 indicate exactly when changes in $c_p(T)$ occur due to crystallization and melting: the moment such a process results in a change in crystallinity and hence in a value for $dw^c(T)/dT$, a $c_{p\ excess}(T)$ will occur according to (8). Like the crystallinity, the excess function, too, is highly sensitive to inaccuracies in the measurement.

Figure 15 shows the invariant values as a function of temperature in cooling and heating. Like the DSC curves, these curves also show that the EO copolymers crystallize and melt, and that they do so in virtually the same manner. This proves that the SAXS invariant is highly sensitive to changes in the number of scattering crystallized ethylene units during cooling and heating. In absolute terms the value of the invariant is roughly halved compared with the value in the case of the EP copolymer EJ 207. The curve shape is once again characteristic, see the discussion relating to (12).
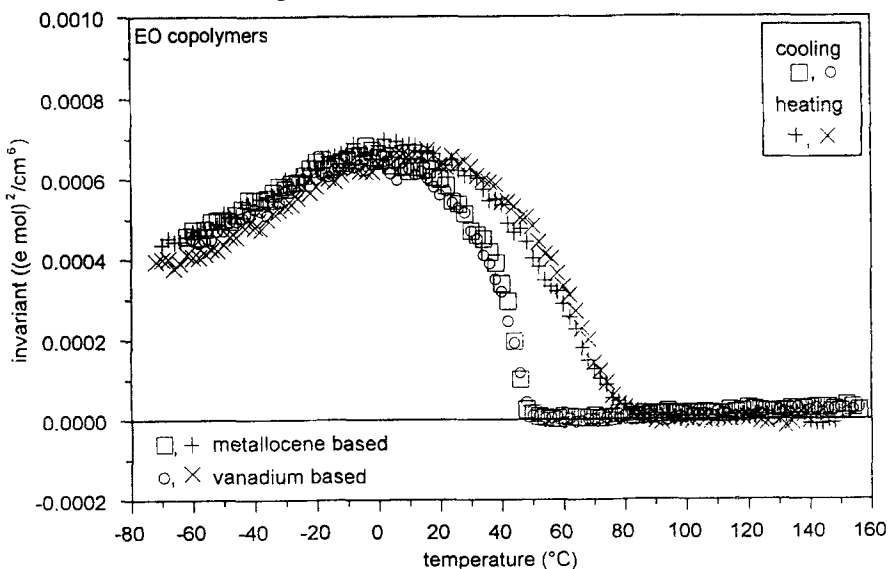

Fig. 15 SAXS invariant curves for cooling and subsequent heating at 20°C min^{-1} in between approx. −70°C and approx. 150°C for two EO copolymers, produced with the aid of different catalyst systems

3.5 Homogeneous copolymers having densities of between 855 and approx. 870 kg m^{-3}

The higher their comonomer content, the lower the temperatures at which the copolymers crystallize and melt. For another series of homogeneous EP copolymers – which were produced using the same catalyst under slightly different polymerization conditions – at a propylene content of about 40 mol%, the point was reached where further addition of propylene would leave nothing but a glass transition [1]; alternatively, one might say that if there were any ethylene sequences left which might crystallize, this would be prevented by vitrification. In the case of this type of copolymer there is really no point in discussions about the smallest crystallizable ethylene sequence. In the first place, experimental verification would be impossible in case vitrification interferes with crystallization as just outlined; in the second place, experimental verification strongly depends on the sensitivity of the apparatus used and on whether one is capable of separating the baseline c_p from the excess c_p.

EJ 198 is an example of an EP copolymer having a density of between 855 and 870 kg m^{-3}. Its ethylene content is 69.2 mol%. Figure 16a shows a simulation of the chain microstructure using the Monte Carlo procedure as discussed in section 3.3. Figure 16b shows the analytically calculated sequence length distributions for ethylene and propylene. Figure 16a gives a good impression of the degree to which the propylenes will interfere with the crystallization of the ethylene sequences in the chain segment. This interference will be rather strong because, in contrast with the EP copolymer EJ 207, see Fig. 3, there are also propylene sequences present.

The sample has no WAXS reflections whatsoever above –70°C according to the synchrotron experiments. However, like the EO copolymers in the previous section, this sample too is definitely capable of crystallizing and melting.

Figure 17 shows this in cooling and heating, respectively. Crystallization now starts just above 0°C and continues until the onset of vitrification, just below –50°C. In heating, the melting process starts immediately above the glass transition and ends at about 20°C. In the melt a slight deviation is observable compared with $c_{pa}(T)$, which is probably due to a slight inaccuracy in the measurement. Nevertheless, both crystallization and melting are readily measurable.

In this case, too, the crystallization and melting processes can readily be followed with the aid of SAXS, see the invariant curves as a function of temperature in Fig. 18. There is even a (weak) maximum in the SAXS $I(q,T)$ curves (not shown here). There is excellent agreement between SAXS and DSC as regards the onset of crystallization and the end of melting.

4. Discussion

Quantitative heat capacity measurements on ethylene copolymers with the aid of DSC reveal crystallization, vitrification and melting processes across the entire density range, see Fig. 1 [1, 2, 72]. The heat capacity measurements on

EP−copolymer　　　　　　　　　　　　　　　　EJU 198

Monomer	Symbol	mole(%)	r ($r_e r_p$ = .81)	P	s_n
ethylene	□	69.2	16.374	.678	3.1
propylene	■	30.8	.049	.277	1.4

a

EP−copolymer　　　　　　　　　　　　　　　　EJU 198

$w_{s:e}$

$w_{s:p}$

x_e = .69

x_p = .31

r_e = 16.4

r_p = .049

$r_e r_p$ = .81

b

W_s

s
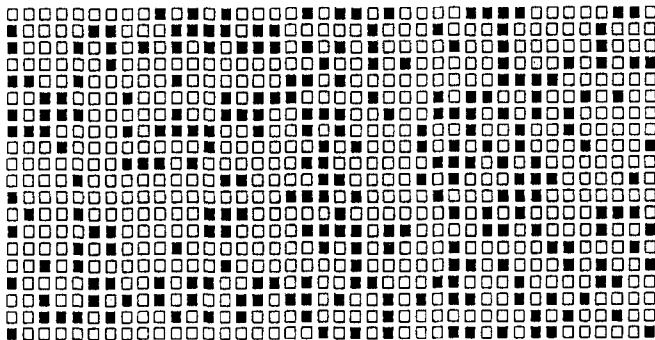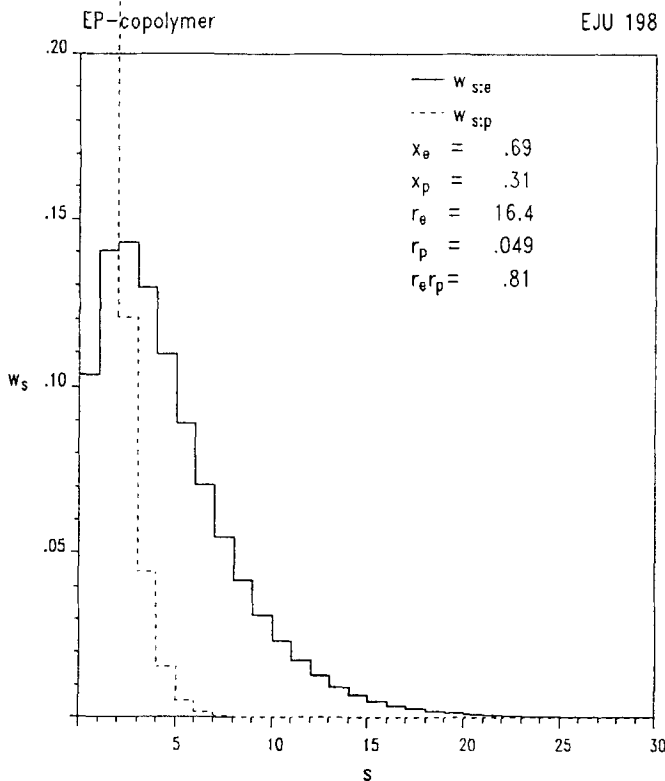
Fig. 16 a) Simulation of a chain segment of the EP copolymer EJ 198. The segment is constructed by linking the lines as in text reading; b) The mass fractions of ethylene in ethylene sequences of length s, $w_{s:e}$, and the mass fractions of propylene in propylene sequences of length s, $w_{s:p}$
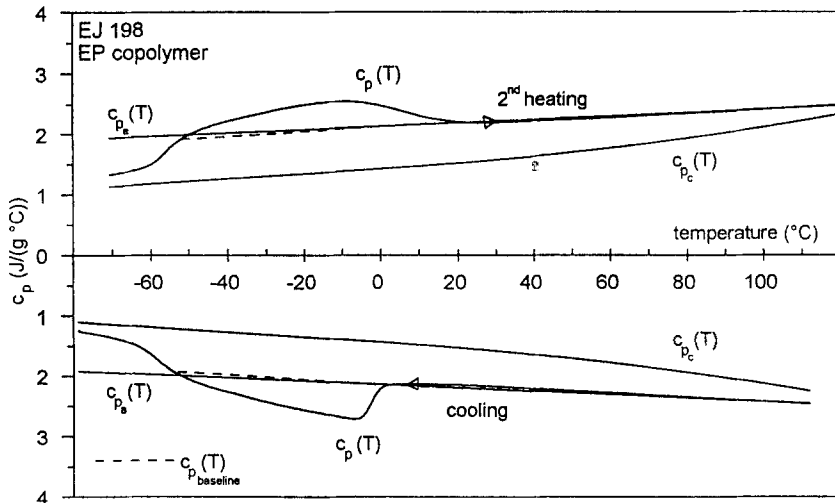
Fig. 17 DSC-7 continuous specific heat capacity curves, $c_p(T)$, at $10°C$ min^{-1} for EJ 198 obtained in cooling (downwards) and subsequent heating (upwards) in between -80 and $120°C$; the reference curves, $c_{pa}(T)$ and $c_{pc}(T)$ and the baseline curves, $c_{pb}(T)$ ($-$ $-$ $-$). Isothermal stays of 5 min, sample mass of 15.310 mg

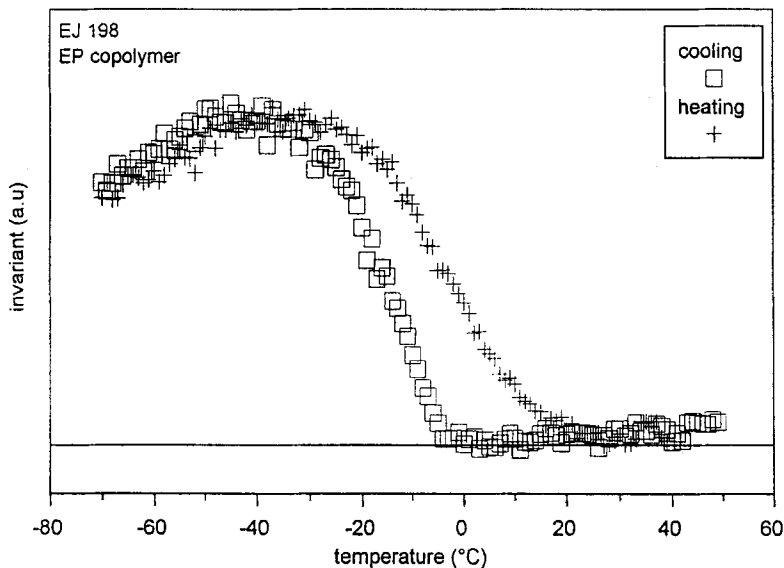**Fig. 18** SAXS invariant curves for cooling and subsequent heating at $20°C$ min^{-1} in between approx. $-70°C$ and approx. $50°C$ for EJ 198

the copolymers were used to calculate the enthalpy values, which, together with the enthalpy reference values for purely amorphous and purely crystalline LPE [69, 76] made it possible to calculate the crystallinity values. In addition, the

baseline and excess heat capacities were determined [72, 75]. The excess values are crucial if the heat capacity measurements are to be used as input into a crystallization model. In this report the simple two-phase model is used for evaluating the DSC results. After a discussion of morphological aspects we shall come back to this model and to the crystallinity concept.

The contribution of time-resolved SAXS-WAXS measurements has proved to be very valuable: due to the high radiation intensity, it was possible for the first time to obtain morphological information about nucleation, crystallization and melting of crystallizable ethylene copolymers of high comonomer content under practical conditions, including conditions often used in DSC measurements.

WAXS measurements reveal that in the case of the samples with the lowest densities no crystalline reflections are observable. This is no doubt due to the limited crystallite dimensions – the lower limit for WAXS is about 50 Å – in combination with the imperfection of the crystal lattice. The demarcation line above which orthorhombic reflections are measurable by WAXS and below which this is impossible under normal measuring conditions lies at a density of roughly 870 kg m^{-3}. The WAXS curves of the ethylene-octene copolymers under review here, with densities of around 870 kg m^{-3}, do seem to contain more information though [30], see the specific shape of the curve in Fig. 11.

For all the samples discussed here, a maximum is observable in the SAXS intensity curve (this maximum is weak in the case of the sample with the lowest density). Apparently there are fluctuations in electron density, whose distance distribution is such that they give rise to a correlation maximum. Given this fact, plus the fact that for copolymers with densities of more than about 870 kg m^{-3} WAXS reflections are possible, we may assume that in those copolymers reasonably perfect crystallites are present. TEM micrographs of the EP copolymer EJ 207 and the two EO copolymers, show that lamellae are indeed present, see also Hwang [23], but that these have not been organized into stacks. This is in contrast with the polyethylenes with much higher densities which were recently studied by [94, 97] with the aid of synchrotron radiation. So in the case of EJ 207 and definitely in the case of copolymers with lower densities, one should not calculate L_c and L_a from L via the crystallinity using a 'direct analysis' of the SAXS intensity curves. In order to be able to calculate 'apparent amorphous dimensions' and 'apparent crystalline dimensions' one should first determine the morphology with the aid of TEM, which enables the scattering intensity to be modelled.

Interesting topics in this connection are the dynamics of reorganization processes such as sliding diffusion [98, 99] upon lamellar thickening of LPE and HDPE and the question whether (and to what degree) thickening occurs in these ethylene polymers under practical measuring conditions, such as during a synchrotron SAXS-WAXS measurement or during a DSC measurement (Fig. 9.3 in

[72]) at scanning rates in the order of 0.2–40°C min⁻¹. In the case of the co-polymers discussed here, sliding diffusion will not occur at these scanning rates, or will occur to only a very low degree, because comonomers such as propylene are likely to considerably hinder the diffusion of ethylene sequences through a crystallite, and comonomers like octene are likely to make such diffusion impossible.

We were initially surprised to find that the invariant values calculated from the SAXS curves were sensitive to crystallization and melting over the entire density range of the copolymers, that is, even below 870 kg m⁻³. Plots of these invariant values as a function of temperature all have a maximum. This is not caused by the maximum at $v^c(T) = 0.5$ for the crystallinity term, $v^c(T)[1 - v^c(T)]$, in the invariant within the two-phase model [94], since $v^c(T)$ remains below 0.4 for all the samples discussed here. The shape of the invariant curve can be explained within the two-phase model with the aid of temperature-dependent crystallinity values and temperature-dependent density reference values. The maximum is the resultant of opposite contributions to the invariant from the crystallinity term and the density term, see the discussion at (12). However, a quantitative description can be given only if for the crystalline phase a density is taken which is lower than that of purely crystalline LPE.

What could be the reason for this? To answer this question, we shall first discuss the general train of events expected to take place during crystallization of copolymers which contain a considerable quantity of comonomer, as reported on here. In the case of such copolymers, upon nucleation and further growth of crystallites comparable ethylene sequences will try to find one another (Flory's equilibrium and exclusion model [11–13]). In principle, the same is true if the comonomer can be included to a certain degree as a defect, as in the case of propylene. However, the 'matching' of comparable ethylene sequences will be only partially successful [4] on account of the statistical linking in the chain of sequences of unequal length due to the polymerization kinetics. At any temperature, the longest ethylene sequences available will preferentially nucleate or grow at a crystal face. As a result, up to a certain distance from such a fixation point the mobility of adjacent chain segments will be reduced. The fact that these adjacent sequences are to some extent fixed means that their crystallization possibilities are limited. In particular when a chain is fixed in several places, its possibilities for additional crystallization as a function of time or, as in this case, upon a decrease in temperature, are limited. Moreover, the chance of success of a certain 'matching' of comparable ethylene sequences also depends on the mobility as such of the chain and its segments, which in its turn is determined by the absolute temperature on the one hand and the distance between the actual temperature and the glass transition temperature on the other. This very general outline explains why, on the one hand, there is a crystal-

lization range in which, in accordance with the ethylene sequence length distribution, the ethylene sequences successively crystallize, the longest ones first and the shortest ones last (the order being reversed in the case of melting) without a perfect matching of sequence lengths being achieved. Due to the hindering influences sketched above, not all sequences will take part in the crystallization process, as a result of which the crystallinity will be lower than calculated according to Flory's equilibrium model. Furthermore, the crystallite dimensions in lateral direction (roughly perpendicular to the sequence direction) will be limited.

So although it is thermodynamically favourable for sequences of comparable length to crystallize into a crystallite in accordance with the Flory model, due to kinetic causes – fixation of chain segments during cooling at 10 and $20°C \, min^{-1}$ (the rates applied here) together with the lower mobility of the chains due to the low crystallization temperature – ethylene sequences of unequal length will be trapped in the same crystallite according to the Kilian model. Given the critical dimensions required for thermodynamic reasons, however, longer ethylene sequences will still on average crystallize sooner than shorter ones. A comparable situation occurs in PVC, where syndiotactic sequences of unequal length form crystallites – probably of the fringed micelle type – with an orthorhombic unit cell [100, 101], the difference being that the lateral dimensions are not limited. This difference is caused by the fact that in the case of PVC the densities of the amorphous and crystalline phases are practically the same, so a crowding problem does not occur.

In the case of densities of about $870 \, kg \, m^{-3}$ and lower, WAXS no longer reveals any reflections. This means that the 'crystallites', which can no longer be made visible with the aid of WAXS but which are responsible for the SAXS invariant (which is caused by fluctuations in electron density) cannot really be of any substantial size, nor can they be perfect, as discussed above. This immediately raises the question of what these 'crystallites' actually are. We may assume that, as their comonomer content increases, copolymers go through various stages. First, copolymers in which ethylene sequences crystallize via folding, resulting in a lamellar morphology [24, 102–106]; next, copolymers in which ethylene sequences crystallize via bundling, resulting in a morphology resembling fringed micelles [Ref. [24] and references therein]; and then copolymers in which ethylene sequences crystallize in clusters [107]. Ultimately, copolymers will crystallize at the glass transition with minimum conformational changes, as described by the cold crystallization model [108]. However, in the case of the ethylene copolymers discussed here, cold crystallization does not occur.

A recent computer simulation via the Monte Carlo method, see Refs [1, 107], illustrates how copolymers with high comonomer contents might crys-

tallize. The simulation, involving fractal-like crystal growth in a 3D morphology, shows clustering of ethylene sequences, with no crystallites to speak of, at any rate no crystallites of appreciable size and degree of perfection. In fact, we should simply speak of crystallized ethylene sequences which have been organized into clusters. The imperfection is also illustrated by the fact that crystallized ethylene units will on average have about three crystallized ethylene neighbour units (in a direction perpendicular to the chain), instead of four as in the case of a perfect orthorhombic crystal lattice. This is also in line with the assumption made earlier that in order to explain the SAXS invariant curve a lower density should be taken for the clusters than for purely (orthorhombic) crystalline LPE. In this sense, one might even speculatively regard clusters as semi-crystalline regions with a relatively high density (but not as high as that of crystalline LPE) and a high (but not 100%) crystallinity. In SAXS experiments these clusters are visible as regions because their electron density is significantly higher than that of their surroundings. A lower density than that of LPE would of course also help to prevent a crowding problem (congestion of chains in the transitional layer from a fringed micelle or cluster to the amorphous phase), just as a limited lateral dimension does [109, 110].

Such a morphology also means that a measurement of crystallinity based on *enthalpy* (DSC) should give lower results than measurements based on the *number* of crystallized units [107]. Unfortunately, verification of the latter has so far proved to be impossible for the copolymers under review. WAXS is useless in this respect because WAXS, too, is sensitive to the degree of perfection of the crystalline areas – only those crystallized ethylene sequences which give constructive interference contribute to the reflections – so the total number of crystallized units cannot be determined. Moreover, given the agreement in Fig. 9 between WAXS and DSC crystallinities, there is no reason for such an interpretation. For a thorough evaluation, however, data on a series of copolymers are needed.

We shall now come back to the use of the two-phase model and the calculation of the crystallinity. From the measured results it is clear that there are crystallized ethylenes on the one hand and non-crystallized ethylenes and propylenes on the other, so two different states can be distinguished.

Are there any phase regions? SAXS clearly records electron-density fluctuations, even in the copolymer with the lowest crystallinity. So even in this sample there are distinct 'regions', however small. It is in these regions that the crystallized ethylene sequences must be present. The regions are probably not only small and imperfect but also lack a clear boundary (see also 3D impression in Fig. 4 in [107]. For these reasons, we used the term 'clusters'.

The copolymers reported here show that there are a lot of questions with regard to homogeneous copolymers which remain unanswered and that further research is necessary. Such research would first of all require the availability of a

series of well-defined copolymers which vary in comonomer type and content. The chain microstructure of such polymers would then need to be determined, and this is possible only if the polymerization process yields structures which can be fully defined in advance or if these structures can be measured. In the latter case, copolymers with very short ethylene sequences would be required, because, unfortunately, ^{13}C-NMR can only measure the methylene sequences 1 through 5, all longer sequences being pooled. For the EP copolymers discussed here such an analysis of the chain microstructure has been carried out successfully [1, 61], enabling further research on ethylene copolymers in which propylene is the comonomer. Recently the same analysis has been carried out for vanadium-based EO copolymers, including the EO copolymer shown here [67].

As the many questions concerning the crystallization and melting behaviour and the morphology of homogeneous copolymers in relation to the molecular structure of these copolymers are beginning to be answered, we may hope to be able one day to answer similar questions about heterogeneous copolymers. Heterogeneous copolymers have a far more complex molecular structure [1, 8, 9, 32, 111]; LLDPE and VLDPE, for example, are blends [1, 9, 32, 47, 111–113] of molecules which differ greatly in comonomer content, even at the same chain length. VLDPE molecules show exceptional behaviour: they crystallize and melt across a temperature range of about 200°C above the glass transition [1, 35, 72]. Therefore, in VLDPE we expect to find all types of crystallites: lamellae with folded ethylene sequences, fringed micelles with bundled ethylene sequences and clusters with loosely packed ethylene sequences.

6. Conclusions

Quantitative DSC measurements were performed between –70 and 180°C to determine the heat capacity, enthalpy, crystallinity, base-line c_p and excess c_p of homogeneous ethylene-propylene and ethylene-octene copolymers with molar percentages of ethylene between about 70 and 90 at densities between roughly 855 and 900 kg m^{-3}.

Using time-resolved simultaneous SAXS-WAXS-DSC measurements it appeared to be possible to record the morphology at the same cooling and heating rates as used in stand-alone DSC measurements, viz. 10 and 20°C min^{-1}.

Crystalline WAXS reflections were found only in the case of copolymers whose density exceeded, say, 870 kg m^{-3} (i.e. at the lowest comonomer contents).

In cases where crystallinity values could be calculated on the basis of density, WAXS and DSC, these were in agreement.

The SAXS measurements show a long period for all copolymers, which means that in each sample there are electron fluctuations giving rise to a correlation maximum.

The SAXS invariant values as a function of temperature appear to be sensitive to crystallization and melting for all copolymers, the onset of crystallization and the end of melting being in agreement with the DSC results.

The SAXS invariant values show a maximum as a function of temperature, which can be explained from the opposite influences of the crystallinity on the one hand and the difference in electron density between the two phases on the other. It has been found that in order to be able to describe the invariant curves in quantitative terms one must assume the density of the crystalline phase to be lower than that of purely (orthorhombic) crystalline linear polyethylene.

The results suggest that in the copolymers with the highest comonomer contents clusters of loosely packed crystallized ethylene sequences are formed upon cooling. In these clusters the enthalpy is reduced (formation of crystallinity as detected by DSC); the electron density and the density are increased (but not to the point where they equal those of purely crystalline LPE; the increase in electron density gives rise to SAXS invariant values); and the absence of crystalline WAXS reflections is explained as being due to the clusters being too small and/or imperfect to give constructive interference.

Though based on totally different homogeneous catalyst systems (vanadium and metallocene based), the ethylene copolymers are similar in terms of crystallization and melting behaviour. This suggests that they do not differ much in ethylene and octene sequence length distribution, and the same must be true for the chain propagation probabilities of ethylene and octene addition during polymerization.

* * *

References

1 V. B. F. Mathot, Ch. 9: 'The Crystallization and Melting Region' in: 'Calorimetry and Thermal Analysis of Polymers', V.B.F. Mathot (Ed.), Hanser Publishers, München 1994, p. 231.
2 V. B. F. Mathot, 'Crystallization and Melting of Linear, Branched and Copolymerized Polyethylenes as Revealed by Fractionation Methods and DSC' in: 'New Advances in Polyolefins', T. C. Chung (Ed.), Plenum Press, 1994, p. 121.
3 R. K. Bayer, Colloid & Polymer Sci., 269 (1991) 421; 270 (1992) 331; 272 (1993) 910.
4 H. G. Kilian, in: 'Thermal Analysis and Calorimetry in Polymer Physics', V. B. F. Mathot (Ed.), Special issue Thermochimica Acta, 238 (1994) 113.
5 R.G. Alamo and L. Mandelkern, in: 'Thermal Analysis and Calorimetry in Polymer Physics', V. B. F Mathot (Ed.), Special issue Thermochimica Acta, 238 (1994) 155.
6 B. Wunderlich, 'Macromolecular Physics, Vol. 3: Crystal Melting'; Academic Press, New York 1980.
7 S.-D. Clas, K. E. McFaddin, K. E. Russell, M. V. Scammel-Bullock and I. R. Peat, J. Polym. Sci.: Part A: Polym. Chem., 25 (1987) 3105.
8 S. Hosoda, Polym. J., 20 (1988) 383.

 9 G. Bodor, H. J. Dalcomo and O. Schröter, Colloid & Polymer Sci., 267 (1989) 480.

10 C. G. Vonk and H. Reynaers, Polym. Commun., 31 (1990) 190.

11 P. J. Flory, J. Chem. Phys., 15 (1947) 684.

12 P. J. Flory, Trans. Faraday Soc., 51 (1955) 848.

13 P. J. Flory, and L. Mandelkern, J. Polym. Sci., 21 (1956) 345.

14 K. Casey, C.T. Elston and M. K. Phibbs, Polym. Letters, 2 (1964) 1053.

15 I. J. Bastien, R.W. Ford and H. D. Mak, Polym. Letters, 4 (1966) 147.

16 C. T. Elston, Can. Pat. No. 984,213, 1967.

17 K. K. Dohrer, L. G. Hazlitt and N. F. Whiteman, J. Plast. Film Sheeting, 4(3) (1988) 214.

18 H. Sinn and W. Kaminsky, Angewandte Chemie, International Edition, Engl., 19 (1980) 390.

19 C. S. Speed, SPE Polyolefins, VII (1991) 46.

20 K. W. Swogger, Proceedings of the 1992 Specialty Polyolefins Conference, Schotland Business Research, Sept., (1992) 157.

21 B. C. Childress, Worldwide Metallocene Conference MetCon '94, Houston, USA, 1994.

22 L. Woo, M. T. K. Ling and S. P. Westphal, in: Proceedings of the Am. Chem. Soc., Div. Polym. Mat.: Sci. and Eng., 71, Fall Meeting, Washington 1994, p. 611.

23 Y-C. Hwang, S. Chum, R. Guerra and K. Sehanobish, Antec 94 SPE Conference Proceedings, Vol III (1994) 3414.

24 B. Wunderlich: 'Macromolecular Physics, Vol. 1: Crystal Structure, Morphology, Defects', Academic Press, New York 1973.

25 B. Wunderlich 'Macromolecular Physics, Vol. 2: Crystal Nucleation, Growth, Annealing'; Academic Press, New York 1976.

26 'Calorimetry and Thermal Analysis of Polymers', V. B. F. Mathot (Ed.); Hanser Publishers, München 1994.

27 V. B. F. Mathot, M. F. J. Pijpers, R. L. Scherrenberg and W. Bras, in: Proceedings of the 23rd NATAS Conference; J. B. Enns (Ed.), Toronto 1994, p. 150;
V. B. F. Mathot, R. L. Scherrenberg, M. F. J. Pijpers and W. Bras, in: Polym. Prepr. of the Am. Chem. Soc., Div. Polym. Chem., 36(1), ACS Meeting 'Advances in Crystalline Polymers', California Meeting, Anaheim 1995, p. 302.

28 W. Bras, G. E. Derbyshire, A. J. Ryan, G. R. Mant, A. Felton, R. A. Lewis, C. J. Hall and G. N. Greaves, Nucl. Instrum. Meth. Phys. Res. A, 326 (1993) 587.

29 W. Bras, G. E. Derbyshire, S. M. Clark, A. J. Ryan and J. Cooke, submitted to the Journal of Applied Crystallography.

30 D. C. McFaddin, K. E. Russell, Gang Wu and R. D. Heyding, J. Polym. Sci.: Part B: Polym. Phys., 31 (1993) 175.

31 C. G. Vonk, J. Appl. Cryst., 6 (1973) 148.

32 V. Mathot, in: 'Polycon '84 LLDPE', The Plastics and Rubber Institute, London 1984, p. 1;
V. B. F. Mathot, H. M. Schoffeleers, A. M. G. Brands and M. F. J. Pijpers, in: 'Morphology of Polymers', B. Sedláček (Ed.), Walter de Gruyter & Co., Berlin–New York 1986, p. 363.

33 V. B. F. Mathot and M. F. J. Pijpers, Polymer Bulletin, 11 (1984) 297.

34 V. Mathot, T. Pijpers and W. Bunge, in: Polym. Prepr. of the Am. Chem. Soc., Div. Polym. Chem., ACS Meeting 'Recent Advances in Polyolefin Polymers', 67, Fall Meeting, Washington 1992, p. 143.

35 V. B. F. Mathot and M. F. J. Pijpers, J. Appl. Polym. Sci., 39(4) (1990) 979.

36 V. Mathot, M. Pijpers, J. Beulen, R. Graff and G. van der Velden, in: 'Proceedings of the Second European Symposium on Thermal Analysis 1981 (ESTA2)', D. Dollimore (Ed.), Heyden, London 1981, p. 264.

37 B. K. Hunter, K.E. Russell, M. V. Scammell and S. L. Thompson, J. Polym. Sci.: Polym. Chem. Ed., 22 (1984) 1383.

38 Th. G. Scholte, N. L. J. Meijerink, H. M. Schoffeleers and A. M. G. Brands, J. Appl. Polym. Sci., 29 (1984) 3763.

39 K. Murata and S. Kobayashi, Kobunshi Kagaku, 26 (1969) 536.

40 J. M. Barrales-Rienda and J. M. G. Fatou, Polymer, 13 (1972) 407.

41 J.-H. Hser and S. H. Carr, Polym. Eng. Sci., 19 (1979) 436.

42 V. B. F. Mathot and M. F. J. Pijpers, Polymer Bulletin, 11 (1984) 297.

43 Magill, J. H., in: 'Polymer Handbook' 3rd ed., J. Brandrup, E.H. Immergut (Eds.), Wiley, 1989, p. VI/279.

44 R. G. Alamo, E. K. M. Chan, L. Mandelkern and I. G. Voigt-Martin, Macromolecules, 25(24) (1992) 6381.

45 R. G. Alamo, B. D. Viers and L. Mandelkern, Macromolecules, 26 (1993) 5740.
46 V. B. F. Mathot, in: 'Crystallization of Polymers', M. Dosière (Ed.), NATO ASI-C Series 'Mathematical and Physical Sciences', 1993, p. 102.
47 R. A. C. Deblieck and V. B. F. Mathot, J. Mater. Sci. Lett., 7 (1988) 1276.
48 F. M. Mirabella, Jr., S. P. Westphal, P. L. Fernando, E. A. Ford and J. G. Williams, J. Polym. Sci.: Part B: Polym. Phys., 26 (1988) 1995.
49 J. van Ruiten and J. W. Boode, Polymer, 33(12) (1992) 2549.
50 R. B. Richards, J. Appl. Chem., 1 (1951) 370.
51 C. H. Baker and L. Mandelkern, Polymer, 7 (1966) 71.
52 C. G. Vonk, in: 'Proceedings Golden Jubilee Conference Polyethylenes', The Plastics and Rubber Institute, Chameleon Press Ltd., London 1983, p. D2.1.
53 R. Alamo, R. Domszy and L. Mandelkern, J. Phys. Chem., 88 (1984) 6587.
54 F. J. Baltá Calleja and C. G. Vonk: X-ray Scattering of Synthetic Polymers. Polymer Science Library 8, Elsevier, Amsterdam 1989.
55 C. G. Vonk and H. Reynaers, Polym. Commun., 31 (1990) 190.
56 C. G. Vonk, J. Polym. Sci.: Part C, 38 (1972) 429.
57 J. Martinez de Salazar and F.J. Baltá Calleja, J. Cryst. Growth, 48 (1979) 283.
58 C. France, P. J. Hendra, W. F. Maddams and H. A. Willis, Polymer, 28 (1987) 710.
59 J. Martinez-Salazar, M. Sánchez Cuesta and F. J. Baltá Calleja, Colloid & Polymer Sci., 265 (1987) 239.
60 J. A. Parker, D. C. Bassett, R. H. Olley and P. Jaaskelainen, Polymer, 35(19) (1994) 4142.
61 V. B. F. Mathot, Ch. C. M. Fabrie, G. P. J. M. Tiemersma-Thoone and G. P. M. van der Velden, in: 'Proceedings Int. Rubber Conf. (IRC)', Kyoto, October 15–18, 1985, p. 334.
62 V. B. F. Mathot and Ch. C. M. Fabrie, J. Polym. Sci.: Part B: Polym. Phys., 28 (1990) 2487.
63 V. B. F. Mathot, Ch. C. M. Fabrie, G. P. J. M. Tiemersma-Thoone and G. P. M. van der Velden, J. Polym. Sci.: Part B: Polym. Phys., 28 (1990) 2509.
64 H. N. Cheng, Macromolecules, 17 (1984) 1950.
65 H. N. Cheng and M. A. Bennett, Makromol. Chem., 188 (1987) 135.
66 J. C. Randall, Rev. Macromol. Chem. Phys., C29(2 & 3) (1989) 201.
67 V. B. F. Mathot, G. P. J. M. Tiemersma-Thoone, G. Evens, J. Pijpers and J. Beulen, to be published.
68 V. B. F. Mathot, Ch. C. M. Fabrie, G. P. J. M. Tiemersma-Thoone and G. P. M. van der Velden, to be published.
69 V. B. F. Mathot, Polymer, 25 (1984) 579. Errata: Polymer, 27 (1986) 969.
70 B. Wunderlich and G. Czornyj, Macromolecules, 10(5) (1977) 906.
71 J. J. Maurer, Rubber Chem. Technol., 38 (1965) 979.
72 V. B. F. Mathot, Ch. 5: 'Thermal Characterization of States of Matter' in: 'Calorimetry and Thermal Analysis of Polymers', V. B. F. Mathot (Ed.); Hanser Publishers, München 1994, p. 105.
73 V. B. F. Mathot and M. F. J. Pijpers, J. Thermal Anal., 28 (1983) 349.
74 M. Dole and B. Wunderlich, J. Polym. Sci., 24 (1957) 139.
75 V. B. F. Mathot and M.F.J. Pijpers, Thermochim. Acta, 151 (1989) 241.
76 The ATHAS Data Bank 1980: U. Gaur, S.-F. Lau, H.-C. Shu, B. B. Wunderlich, A. Mehta, B. Wunderlich, J. Phys. Chem. Ref. Data, 10 (1981) 89, 119, 1001; 11 (1982) 313, 1065; 12 (1983) 29, 65, 91; Update: M. Varma-Nair and B. Wunderlich, J. Phys. Chem. Ref. Data, 20(2) (1991) 349;
The Eight ATHAS Report - 1995.
77 B. Wunderlich: 'Thermal Analysis', Academic Press, Inc., San Diego 1990.
78 M. Alsleben, C. Schick and W. Mischok, Thermochim. Acta, 187 (1991) 261.
79 P. P. A. Smit, Rheol. Acta, 5 (1966) 277.
80 F. R. Schwarzl, Rheol. Acta, 5 (1966) 270.
81 G. Kraus, Adv. Polym. Sci., 8 (1971) 155.
82 L. C. E. Struik, in: 'Physical Aging in Amorphous Polymers and Other Materials', Elsevier, Amsterdam 1978.
83 B. Wunderlich, in: ''Thermal Characterization of Polymeric Materials'', E. A. Turi (Ed.), Academic Press, Inc., Orlando, Florida 1981, p. 92.
84 C. G. Vonk and A. P. Pijpers, J. Polym. Sci.: Polym. Phys. Ed., 23 (1985) 2517.
85 S. Z. D. Cheng, M.-Y. Cao and B. Wunderlich, Macromolecules, 19 (1986) 1868.

86 H. Suzuki, J. Grebowicz and B. Wunderlich, Brit. Polym. J., 17 (1986) 1.
87 S. Z. D. Cheng and B. Wunderlich, Macromolecules, 20 (1987) 1630.
88 L. C. E. Struik, in ref. 82 and in a number of papers: Polymer, 28 (1987) 1521, 1534; Polymer, 30 (1989) 799, 815.
89 S. Z. D. Cheng and B. Wunderlich, Thermochim. Acta, 134 (1988) 161.
90 S. Z. D. Cheng, R. Pan and B. Wunderlich, Makromol. Chem., 189 (1988) 2443; S. Z. D. Cheng and B. Wunderlich, Thermochim. Acta, 134 (1988) 161; see also a number of papers by S. Z. D. Cheng and B. Wunderlich
91 L. Mandelkern, R. G. Alamo and M. A. Kennedy, Macromolecules, 23 (1990) 4721.
92 C. Schick and E. Donth, Physica Scripta, 43 (1991) 423.
93 P. Cebe and P. P. Huo, in: 'Thermal Analysis and Calorimetry in Polymer Physics', V.B.F. Mathot (Ed.), Special issue Thermochimica Acta, 238 (1994) 229.
94 A. J. Ryan, W. Bras, G. R. Mant and G. E. Derbyshire, Polymer, 35(21) (1994) 4537.
95 P. R. Swan, J. Polym. Sci., 56 (1962) 403.
96 H. Wilski, Kunststoffe, 54 (1964) 10, 90.
97 M. Peeters: 'Crystallization and Melting Behaviour of Homogeneous Copolymers of Ethene and 1-Octene', Ph.D. Thesis, Katholieke Universiteit Leuven, Belgium 1995.
98 M. Hikosaka, Polymer, 28 (1987) 1257.
99 M. Hikosaka, Polymer, 31 (1990) 458.
100 R. L. Scherrenberg: 'The Structural Aspects of Suspension Poly Vinyl Chloride', Ph.D. Thesis, Katholieke Universiteit Leuven, Belgium 1992.
101 R. L Scherrenberg, Macromolecules, 26(16) (1993) 4118.
102 D. C. Bassett: Principles of Polymer Morphology. Cambridge University Press, 1981;A.S. Vaughan and D. C. Bassett, in: Comprehensive Polymer Science, Vol. 2: Polymer Properties, C. Booth and C. Price (Eds.), Pergamon Press, Oxford 1989, p. 415.
103 I. G. Voigt-Martin, Adv. Polym. Sci., 67 (1985) 194.
104 A. Keller, in: 'Integration of Fundamental Polymer Science and Technology', L.A. Kleintjens and P. J. Lemstra (Eds.), Elsevier Applied Science Publishers Ltd, Essex, England 1986, p. 425.
105 M. Dosière, in: 'Handbook of Polymer Science and Technology', Vol. 2, N.P. Cheremisinoff (Ed.), Marcel Dekker, New York 1989, p. 367.
106 I. G. Voigt-Martin and L. Mandelkern, J. Polym. Sci.: Part B: Polym. Phys., 27 (1989) 967.
107 J. van Ruiten, F. van Dieren and V. B. F. Mathot in: 'Crystallization of Polymers', M. Dosière (Ed.); NATO ASI-C Series Mathematical and Physical Sciences, 1993, p. 481.
108 B. Wunderlich, J. Chem Phys., 29(6) (1958) 1395.
109 P. J. Flory, J. Amer. Chem. Soc., 84 (1962) 2857.
110 C. G. Vonk, in: 'Integration of Fundamental Polymer Science and Technology', L.A. Kleintjens and P. J. Lemstra (Eds.), Elsevier Applied Science Publishers Ltd, Essex, England 1986, p. 471.
111 P. Schouterden, G. Groeninckx, B. Van der Heyden and F. Jansen, Polymer, 28 (1987) 2099.
112 S. A. Karoglanian and I. R. Harrison, Polym. Mater. Sci. Eng., 61 (1989) 748.
113 F. Defoor: 'Molecular, Thermal and Morphological Characterization of Narrowly Branched Fractions of 1-Octene LLDPE', Ph.D. Thesis, Katholieke Universiteit Leuven, Belgium 1992.